JOURNAL OF PETROLOGY

Journal of Petrology, 2016, Vol. 57, No. 7, 1279–1308
doi: 10.1093/petrology/egw040
Advance Access Publication Date: 19 July 2016
Original Article

OXFORD

Coexisting Early Cretaceous High-Mg Andesites and Adakitic Rocks in the North China Craton: the Role of Water in Intraplate Magmatism and Cratonic Destruction

Qiang Ma[1,2], Yi-Gang Xu[1]*, Jian-Ping Zheng[2]*, William L. Griffin[3], Lu-Bing Hong[1] and Liang Ma[1]

[1]State Key Laboratory of Isotope Geochemistry, Guangzhou Institute of Geochemistry, Chinese Academy of Sciences, Guangzhou 510640, China; [2]State Key Laboratory of Geological Processes and Mineral Resources, School of Earth Sciences, China University of Geosciences, Wuhan 430074, China; [3]ARC CoE for Core to Crust Fluid Systems/GEMOC, Macquarie University, NSW 2109, Australia

*Corresponding authors. E-mail: yigangxu@gig.ac.cn and jpzheng@cug.edu.cn

Received May 28, 2015; Accepted June 15, 2016

ABSTRACT

High-Mg andesites (HMAs) and adakitic rocks are purported to occur exclusively in subduction zones in the modern Earth. In the North China Craton, early Cretaceous HMAs and adakitic dacites were erupted in a continental setting, apparently unrelated to subduction given their location distal (>1000 km) to the trench at that time. Here we report petrological, mineralogical and geochemical data for these rocks with the aim of constraining their petrogenesis and elucidating the role of water in intraplate magmatism and cratonic destruction. The HMAs can be subdivided into olivine (Ol-)HMAs and clinopyroxene (Cpx-)HMAs. The former have high MgO (>9·8 wt %) and Mg# (>71), with rare high-Fo (up to 91) olivine phenocrysts, corresponding to (near-)primary magmas that equilibrated with mantle peridotite. The latter have moderate MgO (7·8–8·8 wt %) and Mg# (mostly <70) and low-Fo (mostly < 83) olivine phenocrysts. The Cpx-HMAs are interpreted as magmas differentiated from the Ol-HMAs by olivine-dominated fractionation at lower-crust levels. P–T–X_{H2O} estimations show that the primary HMAs are melts of shallow (1·1–1·2 GPa), hot (~1250°C) and wet ($H_2O > 3$ wt %) lithospheric mantle. The coexisting adakitic dacites are hydrous ($H_2O \geq 5$ wt %) magmas with high SiO_2 (>63 wt %), Sr/Y ratios (≥39) and Yb_{SN} (source-normalized), low $(Sm/Yb)_{SN}$, and negligible Eu anomalies. They also have unradiogenic whole-rock Nd [$\varepsilon_{Nd}(t) = -19$ to -9] and zircon Hf [$\varepsilon_{Hf}(t) = -23$ to -21] isotopic compositions consistent with derivation by melting of ancient lower crust at depths < 40 km. Melting may have been induced by heating and addition of H_2O from underplated HMAs. Mixing between Cpx-HMAs and low-Mg adakitic dacites in magma chambers produced high-Mg adakitic rocks. The petrogenetic model presented here explains the occurrence of intraplate HMAs and adakitic magmas elsewhere in the North China Craton. The P–T–X_{H2O} conditions inferred for HMA generation imply that the subcontinental lithospheric mantle beneath the craton was hot and hydrous in the early Cretaceous, which may have triggered the destruction of the cratonic root. The occurrence of young HMAs and adakitic rocks in an intraplate extensional environment also casts doubts on the common use of a similar igneous rock association as an indicator of subduction processes in Archean time.

Key words: high-Mg andesites; adakitic rocks; water; intraplate; cratonic destruction

INTRODUCTION

High-magnesium andesites [HMAs; synonymous with the primitive andesite of Kelemen *et al.* (2003) and the primitive magnesian andesite of Grove *et al.* (2002)] and related magmas such as 'adakites' (Defant & Drummond, 1990; Martin, 1999; Martin *et al.*, 2005) have attracted increasing attention even though they are volumetrically minor in the modern Earth. HMAs are defined as andesites with high MgO [>5 wt %, Tatsumi (2008); or >8 wt %, Crawford *et al.* (1989)] and low FeO^T/MgO (<1·0, where FeO^T is total iron as FeO; Tatsumi, 2008). They share striking compositional similarities with the bulk continental crust (Tatsumi, 2006) and form a recognizable part of the continental crust as sanukitoids in Archean cratons (Shirey & Hanson, 1984). Their origin thus provides insights into the formation of continental crust on Earth (Kelemen *et al.*, 2003; Tatsumi, 2006). Previous petrological, geochemical and experimental studies (e.g. Tatsumi, 1982, 2006; Crawford *et al.*, 1989; Yogodzinski *et al.*, 1995; Shimoda *et al.*, 1998; Grove *et al.*, 2002; Wood & Turner, 2009; Weaver *et al.*, 2011; Weber *et al.*, 2012) have suggested that HMA magmas can be generated by melting of strongly hydrated mantle peridotite or by interaction of slab-derived melts with an ultramafic mantle wedge. Sufficient supply of hydrous components (Grove *et al.*, 2012) and a high geotherm in the mantle wedge (Crawford *et al.*, 1989; Tatsumi, 2006) are two key factors in the generation of HMAs in subduction zones.

Originally, adakites were defined as a group of intermediate–felsic igneous rocks found in modern subduction zones; they are characterized by high Sr/Y (>40) and La/Yb (>20), depletion in Nb–Ta relative to light rare earth elements (LREE) and large ion lithophile elements (LILE), and absence of obvious Eu anomalies; they are proposed to be a product of melting of subducted basaltic oceanic crust that has been transformed to eclogite (Defant & Drummond, 1990). As they are compositionally similar to the Archean tonalite–trondhjemite–granodiorite (TTG) suites (Martin, 1999) that make up a large proportion of the continental crust, clarification of their origins can potentially improve our understanding of crustal evolution (Martin *et al.*, 2005; Castillo, 2006, 2012). Currently, the term adakite is used for a wide variety of igneous rocks, whose sole common feature is high Sr/Y and La/Yb ratios (Castillo, 2006, 2012; Moyen, 2009). This loose geochemical definition may not be appropriate; the term adakite must be restricted to true slab melt, and other rock types with adakitic signatures should be termed adakitic rocks (Castillo, 2006, 2012; Ma *et al.*, 2015). Various models have been proposed to account for the origin of intermediate–felsic igneous rocks with adakitic signatures (Martin *et al.*, 2005; Castillo, 2006, 2012; Lee *et al.*, 2007; Richards & Kerrich, 2007), with general emphasis on melting depth (Defant & Drummond, 1990; Gao *et al.*, 2004), inheritance from source composition (Qian & Hermann, 2013; Ma *et al.*, 2015) and magma generation processes (Castillo *et al.*, 1999; Chen *et al.*, 2013; Chiaradia, 2015).

The bulk of HMAs and adakitic rocks in the modern Earth are closely associated with subduction environments, which provide possibilities for both hydrous melting of the mantle and high-pressure melting of subducted oceanic crust. In recent years, igneous rocks with compositions similar to HMAs and adakitic rocks have been identified in intra-continental settings, such as in the North China Craton (NCC) (e.g. Zhang *et al.*, 2003; Gao *et al.*, 2004; Xu *et al.*, 2008; Ma *et al.*, 2015). Because these magmas have no obvious relationship to a subduction process (e.g. >1000 km away from a contemporary subduction zone), alternative models have been put forward. These intraplate high-Mg diorites or andesites (hereafter HMAs) have geochemical characteristics typical of partial melts formed in the crust (e.g. high SiO_2, enrichment in LILE, and depletion in Nb and Ta) as well as in the mantle (e.g. high MgO, Ni and Cr), leading to a popular model involving interaction of melts, derived from foundered lower crust, with mantle peridotite as they ascended (Xu *et al.*, 2008). However, the formation of these HMAs may also have involved mixing of felsic and basaltic magmas (Zhang & Shao, 2008; Chen *et al.*, 2013) or assimilation of ultramafic rocks at crustal depths (Qian & Hermann, 2010); this new model questions their relevance to delamination and melt–peridotite interaction processes. Melting of lithospheric mantle metasomatized by slab melts has also been proposed for the origin of HMAs in the northern margin of the NCC (Zhang *et al.*, 2003). The debates surrounding their petrogenesis are mainly caused by the ambiguity of the geochemical evidence and the lack of studies on primary HMA magmas that have equilibrated with mantle peridotite (e.g. Zhang *et al.*, 2003). Moreover, the roles of H_2O and high temperatures, two crucial factors in the generation of HMA melts in modern arcs (Parman & Grove, 2004; Tatsumi, 2008; Grove *et al.*, 2012), have not been fully considered in these models, probably owing to lack of appropriate thermobarometers and hygrometers. The high-Mg diorites in the NCC contain abundant hydrous minerals [e.g. up to 40% amphibole; Qian & Hermann (2010); Chen *et al.* (2013)], indicative of H_2O-rich magmas and involvement of hydrous components in their source.

Adakitic magmas in continental settings were originally inferred to be the products of a thickened or foundered lower crust (Xu *et al.*, 2002; Chung *et al.*, 2003; Gao *et al.*, 2004). These premises are built on experiments and modeling of a mid-ocean ridge basalt (MORB)-like source, which show that adakitic geochemical signatures can be produced by high-pressure melting (≥1·5 GPa, Defant & Drummond, 1990; Xiong *et al.*, 2005; Nair & Chacko, 2008). Recent studies have highlighted the importance of source inheritance in the formation of intraplate adakitic magmas (Qian & Hermann, 2013; Ma *et al.*, 2015) and proposed that the Mesozoic adakitic rocks in the NCC were generated at depths <40 km (Ma *et al.*, 2012, 2015). Melting of the nearly

anhydrous and essentially refractory lower crust of the craton can be attributed to heating by episodic underplating of basaltic magma (e.g. Yang & Li, 2008; Ma *et al.*, 2015) and/or by thinning of the lithosphere and upwelling of the asthenosphere (Yang *et al.*, 2008). However, herein lies a problem: models of heat transfer show that high-temperature basalts emplaced into the base of the crust cannot provide enough heat to melt mafic lower crust (even if it is amphibolite) extensively (Annen & Sparks, 2002; Annen *et al.*, 2006), because of the high dehydration-melting temperature of amphibole in mafic rocks (~950°C). Thus, the possibility of crustal melting involving the presence of a free H_2O phase should be considered along with the question of where the water comes from.

To address the petrogenesis of intraplate HMAs and adakitic rocks, we present a combined petrological, mineralogical and geochemical study of these two igneous rock types coexisting in the Liaodong Peninsula in the NCC. The P–T–X_{H2O} conditions for generating HMA magmas are estimated using the thermobarometer developed by Lee *et al.* (2009) and hygrometer–barometer developed by Wood & Turner (2009). Based on these data, we elucidate the importance of water in the generation of intraplate HMA and adakitic magmas and illustrate the probable geodynamic implications of these rocks.

GEOLOGICAL SETTING

The NCC (Fig. 1a) is one of the oldest Archean cratons in the world and preserves ≥3·8 Ga crustal remnants (Liu *et al.*, 1992). It experienced a series of tectono-thermal events in the late Archean and Paleoproterozoic, and stabilized in the late Paleoproterozoic (~1·85 Ga; Zhao *et al.*, 2001). From the late Paleoproterozoic (~1·85 Ga) to the Paleozoic (~250 Ma) this block was stable without significant tectono-thermal events (except emplacement of minor Ordovician kimberlites) and was covered by a thick sequence of sediments. The NCC was affected by subduction and collision with surrounding blocks during Phanerozoic time (Windley *et al.*, 2010), including the Paleozoic southward subduction of the Paleo-Asian oceanic plate (Xiao *et al.*, 2003), the Triassic deep subduction of the Yangtze continental crust (Li *et al.*, 1993) and the Mesozoic–Cenozoic (and still continuing) subduction of the (Paleo-)Pacific plate (Müller *et al.*, 2008; Xu, 2014). As a result of the first two subduction and/or collision episodes, the NCC was amalgamated with the Siberian and South China blocks, leading to the formation of the Central Asian Orogenic Belt to the north and the Qingling–Dabie–Sulu Orogenic Belt to the south, respectively. Studies of xenoliths and separated minerals from Paleozoic kimberlites have revealed that the NCC had a cold (~40 mW^{-2}), thick (~200 km) and ancient (>2·5 Ga) cratonic lithospheric mantle at that time (Griffin *et al.*, 1998; Xu, 2001; Gao *et al.*, 2002; Zheng *et al.*, 2006). In contrast, the lithospheric mantle beneath the eastern NCC in the Cenozoic was warmer (~80 mW m^{-2}), thinner (60–80 km), younger and more fertile (Xu *et al.*, 1995; Menzies & Xu, 1998; Xu *et al.*, 1998; Xu, 2001; Gao *et al.*, 2002; Wu *et al.*, 2003; Zheng *et al.*, 2006). The eastern part of the NCC appears to have lost its lithospheric keel (>100 km) during the Mesozoic and Cenozoic, and represents the best example of craton-root destruction (Menzies *et al.*, 1993; Griffin *et al.*, 1998; Xu, 2001; Carlson *et al.*, 2005; Zheng *et al.*, 2007).

The Liaodong Peninsula is located in the northeastern segment of the NCC (Fig. 1a) and consists of Archean to Paleoproterozoic basement rocks overlain by unmetamorphosed Mesoproterozoic to Paleozoic sediments and Mesozoic to Cenozoic sedimentary and igneous rocks. Mesozoic volcanic and intrusive rocks are widely developed in this region, and mostly formed in the late Jurassic (180–150 Ma) and early Cretaceous (135–117 Ma) (Wu *et al.*, 2005*a*, 2005*b*), although minor Triassic magmatism (233–210 Ma) is also recorded (Yang *et al.*, 2007*a*). The Triassic igneous rocks, including mafic dikes, syenite, diorite, monzogranite and mafic enclaves, probably formed in a post-collisional extensional environment following the assembly of the North China and Yangtze blocks (Yang *et al.*, 2007*a*). The Jurassic intrusive rocks consist of quartz diorite, tonalite, granodiorite and monzogranite and were mainly derived from partial melting of ancient crustal materials (Wu *et al.*, 2005*b*). The tectonic setting in which the Jurassic magmatism of the eastern NCC occurred is controversial. Wu *et al.* (2005*b*) suggested that the Jurassic granites formed in an active compressive continental margin, resulting from subduction of the Paleo-Pacific plate beneath the East Asia plate. Some other studies suggested that the Jurassic magmatism developed in an intraplate contractional environment (e.g. Zhang *et al.*, 2007) or in a post-collisional setting (e.g. Mao *et al.*, 2003; Zhang *et al.*, 2010). The early Cretaceous igneous rocks developed coevally with late Mesozoic metamorphic core complexes (MCC) and occur as plutonic intrusions in the lower plates of the complexes and as volcanic rocks in the supra-detachment basins of the MCC (Fig. 1b; Liu *et al.*, 2013). The MCC were the consequence of crustal or lithospheric extension, which was probably induced by collapse of crust over-thickened as a result of earlier orogenic processes (Wang *et al.*, 2012) or by retreat of the subducting Paleo-Pacific plate beneath the East Asia plate (Liu *et al.*, 2013). Although early Cretaceous tectonism in the Liaodong Peninsula was probably related to far-field effects of Paleo-Pacific plate subduction, the contemporary magmatism should be regarded as of intraplate type, considering that this area was too far (>1000 km) from the trench of this subduction system at that time. The intrusions include dolerite, diorite, granodiorite, I- and A-type granite, and syenite. Detailed geochemical and isotopic studies have shown that they were derived from multiple sources, including depleted mantle, enriched lithospheric mantle, ancient lower crust and juvenile crust (Yang *et al.*, 2004, 2006, 2008;

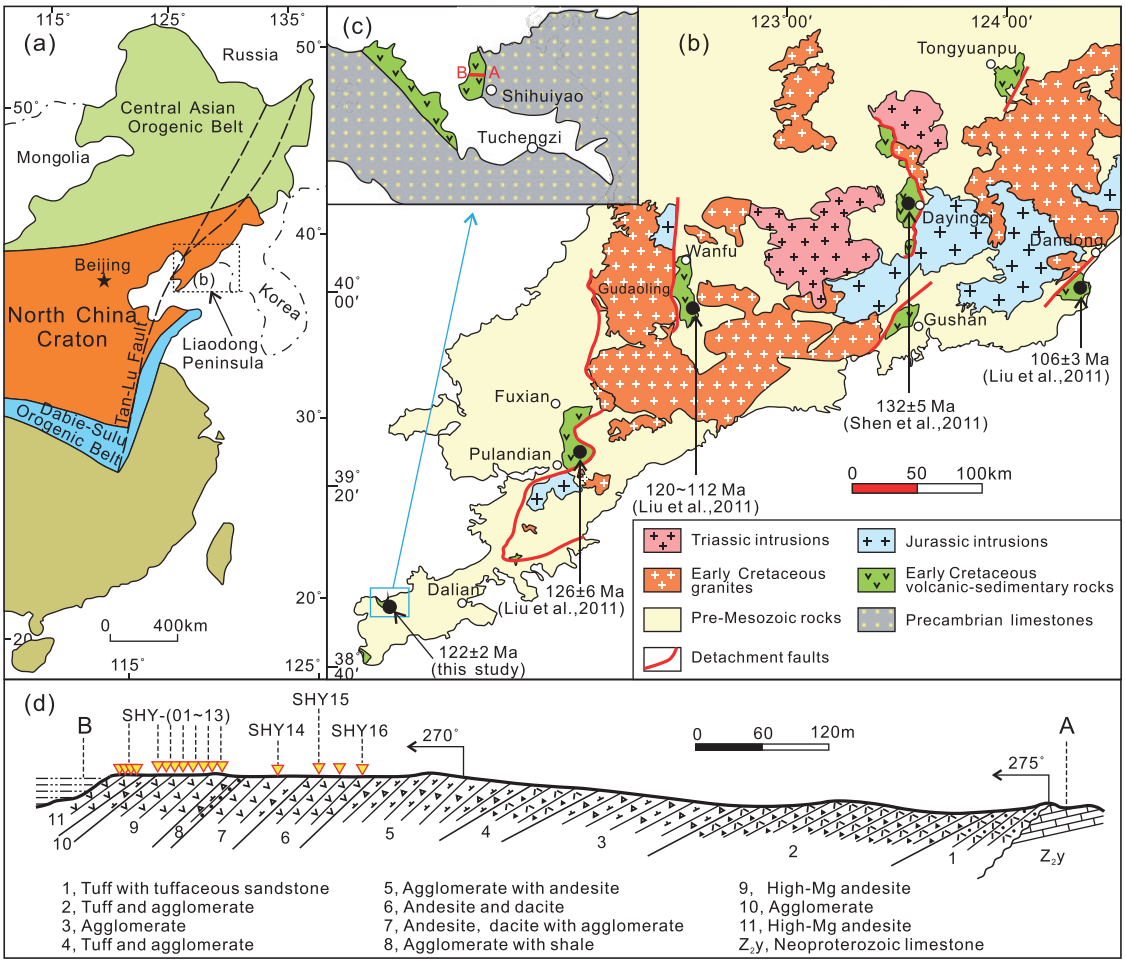

Fig. 1. Simplified geological maps showing (a) major tectonic units of eastern China, (b) Mesozoic magmatism in the Liaodong Peninsula, (c) location and (d) geological cross-section of the Guiyunhua volcanic rocks in the Shihuiyao area. The structural outline and distribution of Mesozoic magmatism in the Liaodong Peninsula in (b) are modified from Liu *et al.* (2013) and Yang *et al.* (2007*a*), respectively. The U–Pb ages of zircons from the Guiyunhua volcanic rocks are from Liu *et al.* (2011), Shen *et al.* (2011) and this study.

Wu *et al.*, 2005*a*). The volcanic rocks, including andesite, dacite, rhyolite, volcanic breccia and tuff, are termed the Guiyunhua volcanic rocks (K_1g; LBGMR, 1989). Previous field and geochronological studies have shown that the volcanic rocks were erupted in early Cretaceous times (132–106 Ma) and were interlayered with lacustrine sediments in fault-bounded extensional basins.

PETROGRAPHY

Samples of the Guiyunhua volcanic rocks, including HMAs (see 'Whole-rock chemistry', below) and dacites, were collected from the Shihuiyao–Dachaokou section near Dalian City (Fig. 1c and d). The HMAs are porphyritic with phenocrysts of euhedral olivine, clinopyroxene and rare orthopyroxene in a groundmass of fine-grained plagioclase, clinopyroxene and minor magnetite. They are phenocryst-poor (<11%; Table 1) andesites, characterized by a lack of plagioclase phenocrysts (Fig. 2a and b), thus resembling sanukitoids from the Setouchi volcanic belt, southwestern Japan (Tatsumi, 2006). Based on modal composition, these HMAs can be subdivided into Ol-HMAs with olivine phenocrysts more abundant than pyroxene phenocrysts (Fig. 2a) and Cpx-HMAs with olivine phenocrysts less abundant than pyroxene (Fig. 2b). Orthopyroxene is found only in Ol-HMAs. Unlike the HMAs, the Guiyunhua dacites (Fig. 2c) are phenocryst-rich (>25%; Table 1) with plagioclase, amphibole and clinopyroxene phenocrysts, in decreasing order of abundance. Amphibole phenocrysts are euhedral and are commonly transformed at the rims into a fine-grained association of pyroxene, plagioclase and opaque oxides (Fig. 2c). The groundmass consists of fine-grained plagioclase, K-feldspar, quartz, clinopyroxene and magnetite.

ANALYTICAL METHODS

Geochemical data presented here include mineral and whole-rock compositions, Sr–Nd isotopes and zircon U–Pb and Hf isotopes, which are listed in Tables 1–4.

Major element compositions of minerals were determined by electron microprobe analysis (EPMA) using a

Table 1. Major and trace elements and modal compositions of the early Cretaceous Guiyunhua volcanic rocks in the Liaodong Peninsula

Sample no.:	SHY-01	SHY-02	SHY-03	SHY-04	SHY-05	SHY-06	SHY-07	SHY-08
Rock type:	Cpx-HMA	Ol-HMA	Ol-HMA	Cpx-HMA	Ol-HMA	Cpx-HMA	Cpx-HMA	Cpx-HMA
Major elements (wt %)								
SiO_2	54·21	54·27	54·31	55·55	54·05	52·85	54·12	54·68
TiO_2	0·76	0·71	0·72	0·77	0·72	0·71	0·70	0·75
Al_2O_3	14·24	13·64	13·71	14·66	13·68	13·73	13·30	14·40
$Fe_2O_3^T$	7·05	7·80	7·81	7·19	7·78	7·91	7·49	7·63
MnO	0·10	0·11	0·11	0·09	0·11	0·09	0·09	0·10
MgO	8·63	10·24	9·93	7·50	10·11	8·14	7·99	7·64
CaO	7·74	7·73	7·53	7·61	7·51	6·68	7·09	7·79
Na_2O	3·01	3·00	3·05	3·14	3·00	2·69	2·92	3·09
K_2O	1·35	1·32	1·35	1·45	1·34	2·68	1·37	1·37
P_2O_5	0·16	0·16	0·16	0·17	0·16	0·16	0·15	0·17
LOI	2·67	1·41	1·25	2·30	1·67	4·78	4·70	1·49
Total	99·92	100·39	99·93	100·43	100·13	100·42	99·92	99·12
FeO^T	6·3	7·0	7·0	6·5	7·0	7·1	6·7	6·9
FeO/MgO	0·74	0·69	0·71	0·86	0·69	0·87	0·84	0·90
Mg#	70·8	72·2	71·6	67·4	72·0	67·1	67·9	66·5
Trace elements (ppm)								
Li	11·2	13·2	13·6	11·8	14·8	15·1	27·0	12·6
Be	1·04	0·91	0·89	0·96	1·02	0·94	1·24	1·18
Sc	24·0	21·9	22·2	22·2	22·9	23·3	22·5	24·2
V	185	168	170	173	179	104	73·3	181·9
Cr	612	531	541	524	576	583	551	596
Co	51·9	50·6	46·0	43·9	50·0	42·2	42·2	40·3
Ni	289	295	302	234	303	267	249	307
Cu	68·8	43·5	38·2	70·0	51·5	54·5	54·1	55·8
Zn	71·0	69·6	69·7	63·6	70·1	75·2	65·5	74·2
Ga	18·3	16·8	17·0	17·5	17·9	17·6	17·7	18·8
Rb	34·9	33·3	33·8	38·1	35·3	46·2	14·8	33·6
Sr	468	447	463	455	463	391	441	466
Y	14·9	14·3	15·2	17·7	15·4	15·2	15·4	16·0
Zr	103	93·5	95·4	105	101	98·6	99·9	98·9
Nb	4·91	4·59	4·54	5·27	4·79	4·65	4·87	4·85
Cs	0·85	3·84	3·23	1·18	2·93	0·44	0·31	1·82
Ba	454	451	483	473	440	633	491	469
La	16·5	16·0	16·4	19·7	16·1	15·9	15·6	18·3
Ce	33·2	34·0	34·5	32·7	33·8	31·4	32·1	34·2
Pr	4·27	4·18	4·22	4·80	4·18	4·18	4·04	4·62
Nd	17·5	17·5	18·1	20·5	16·9	16·9	16·2	19·6
Sm	3·59	3·47	3·75	4·18	3·58	3·35	3·30	3·92
Eu	1·14	1·06	1·11	1·22	1·05	1·08	1·01	1·17
Gd	3·25	3·08	3·18	3·69	3·14	3·09	2·93	3·57
Tb	0·47	0·47	0·48	0·55	0·44	0·45	0·43	0·49
Dy	2·68	2·63	2·80	3·18	2·50	2·67	2·46	2·89
Ho	0·51	0·52	0·53	0·60	0·49	0·49	0·47	0·56
Er	1·38	1·40	1·55	1·79	1·35	1·33	1·36	1·54
Tm	0·20	0·20	0·22	0·24	0·19	0·20	0·19	0·24
Yb	1·36	1·27	1·36	1·53	1·28	1·26	1·25	1·52
Lu	0·20	0·20	0·21	0·24	0·19	0·21	0·20	0·23
Hf	2·58	2·55	2·63	2·85	2·38	2·36	2·24	2·66
Ta	0·31	0·32	0·30	0·36	0·29	0·27	0·26	0·29
Pb	7·26	6·94	6·78	9·04	6·94	7·19	7·81	8·34
Th	3·10	3·03	3·07	3·55	2·90	2·86	2·76	3·20
U	0·74	0·92	0·94	0·85	0·87	0·25	0·19	0·89
Modal composition (vol. %)								
Ol	4·2	7·8	5·8	1·6	5·6	3		2·1
Cpx	6·8	3·2	3·8	7·4	2·7	6·4		8·8
Opx	—	—	—	—	—	—		—
Mag	0·1	—	—	0·3	—	—		0·2
Am	—	—	—	—	—	—		—
Pl	—	—	—	—	—	—		—
GM	Pl + Cpx + Mag	Pl + Cpx + Mag	Pl + Cpx + Ol + Mag	Pl + Cpx + Mag	Pl + Cpx + Mag	Pl + Cpx + Mag		Pl + Cpx + Mag

(continued)

Table 1. Continued

Sample no.:	SHY-09	SHY-10	SHY-11	SHY-12	SHY-13	SHY-14	SHY-15	SHY-16
Rock type:	Cpx-HMA	Ol-HMA	Ol-HMA	Ol-HMA	Ol-HMA	Adakitic dacite	Adakitic dacite	Adakitic dacite
Major elements (wt %)								
SiO_2	55·27	54·20	54·19	53·74	54·22	66·06	60·43	67·62
TiO_2	0·72	0·71	0·71	0·70	0·73	0·54	0·55	0·60
Al_2O_3	14·11	13·42	13·48	13·29	13·53	15·55	15·98	15·45
$Fe_2O_3^T$	7·41	7·87	7·62	7·66	7·72	3·75	5·01	3·50
MnO	0·10	0·11	0·11	0·12	0·11	0·10	0·04	0·04
MgO	7·98	9·90	9·60	10·04	9·86	1·98	2·92	1·09
CaO	7·42	7·50	7·58	7·32	7·45	3·79	4·75	1·48
Na_2O	3·12	2·92	3·02	2·96	3·04	4·68	3·02	3·98
K_2O	1·42	1·31	1·35	1·33	1·34	1·94	2·82	3·67
P_2O_5	0·16	0·16	0·16	0·16	0·17	0·18	0·19	0·20
LOI	1·08	1·01	1·05	0·93	0·99	0·98	2·57	1·23
Total	98·79	99·11	98·88	98·23	99·14	99·55	98·28	98·85
FeO^T	6·7	7·1	6·9	6·9	6·9	3·4	4·5	3·1
FeO/MgO	0·84	0·72	0·71	0·69	0·70	1·70	1·55	2·89
Mg#	68·1	71·4	71·4	72·2	71·7	51·2	53·6	38·2
Trace elements (ppm)								
Li			14·5		15·7	25·2	15·5	26·2
Be			0·98		0·97	1·25	1·82	1·91
Sc			22·6		22·9	10·9	11·0	5·7
V			172·1		171·6	89·0	91·3	25·1
Cr			560		576	112	112	19
Co			43·7		43·0	17·5	17·6	23·1
Ni			309		310	53	53	6
Cu			49·0		30·9	17·2	29·8	5·7
Zn			71·8		72·8	60·2	63·3	52·1
Ga			17·7		17·8	17·8	20·0	19·2
Rb			33·5		32·3	40·6	83·6	78·9
Sr			452		448	485	669	647
Y			15·2		14·6	12·4	13·6	12·9
Zr			94·0		94·1	138·5	143·5	175·9
Nb			4·69		4·68	6·28	6·56	12·16
Cs			2·89		3·71	2·67	4·30	1·5
Ba			453		442	797	722	1427·7
La			16·1		16·0	25·0	26·1	48·41
Ce			33·8		34·0	46·8	48·3	88·9
Pr			4·11		4·11	5·63	5·83	9·54
Nd			17·3		17·1	21·5	22·3	33·25
Sm			3·57		3·52	3·74	4·01	5·12
Eu			1·06		1·08	1·08	1·17	1·47
Gd			3·24		3·29	3·15	3·18	3·85
Tb			0·45		0·45	0·41	0·42	0·47
Dy			2·71		2·55	2·26	2·42	2·23
Ho			0·54		0·51	0·43	0·47	0·38
Er			1·50		1·36	1·15	1·29	1·06
Tm			0·22		0·22	0·17	0·20	0·13
Yb			1·39		1·36	1·16	1·22	0·87
Lu			0·20		0·19	0·18	0·18	0·12
Hf			2·56		2·58	3·61	3·69	4·45
Ta			0·31		0·30	0·46	0·44	0·71
Pb			7·40		7·99	25·67	14·25	17·23
Th			3·01		3·09	5·64	5·89	9·88
U			0·91		0·91	1·70	1·66	1·06
Modal composition (vol. %)								
Ol	2·8	5·2	5·0	4·8	6·9	—	—	—
Cpx	5·4	2·6	4·5	2·1	2·7	1·6	1·4	—
Opx	—	—		0·1	0·2	—	—	—
Mag	—	—	—	—	—	—	—	—
Am	—	—	—	—	—	8·1	5·6	9·4
Pl	—	—	—	—	—	15·6	22·5	19·2
GM	Pl + Cpx + Mag	Pl + Cpx + Ol + Mag	Pl + Cpx + Mag	Pl + Cpx + Mag	Pl + Cpx + Ol + Mag	Pl + Kfs + Mag	Pl + Kfs + Mag	Pl + Kfs + Q + Mag

Ol, olivine; Cpx, clinopyroxene; Pl, plagioclase; Mag, magnetite; GM, groundmass.

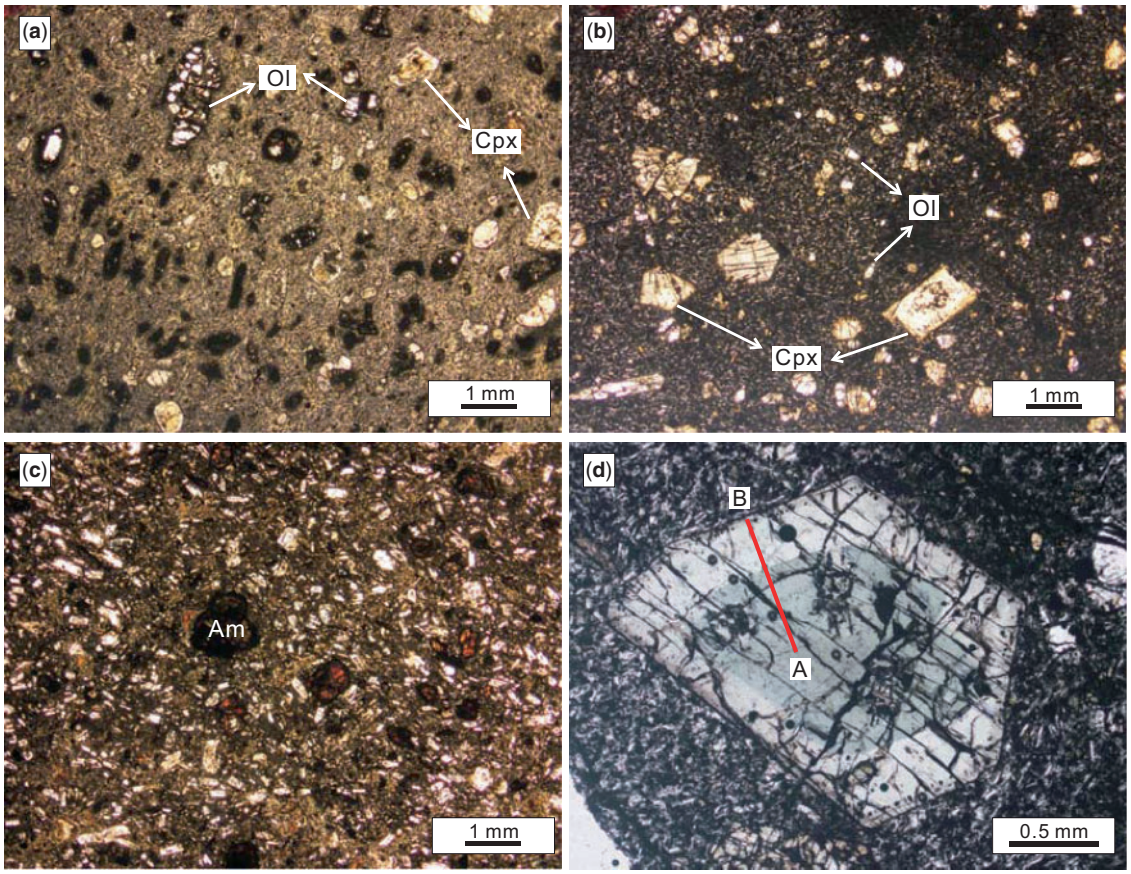

Fig. 2. Photomicrographs (plane-polarized light) showing the petrographic features of representative Ol-HMAs (a), Cpx-HMAs (b), adakitic dacites (c) and green-cored clinopyroxene in Cpx-HMA SHY04 (d) from the Liaodong Peninsula, North China. Line A–B in (d) shows the location of the compositional traverse in Supplementary Data Fig. S2 in Electronic Appendix 4. Cpx, clinopyroxene; Ol, olivine; Am, amphibole.

Table 2. Sr and Nd isotopic compositions of the early Cretaceous Guiyunhua volcanic rocks in the Liaodong Peninsula

Sample no.:	SHY-01	SHY-02	SHY-03	SHY-04	SHY-05	SHY-14	SHY-15	SHY-16
Rock type:	Cpx-HMA	Ol-HMA	Ol-HMA	Cpx-HMA	Ol-HMA	Adakitic dacite	Adakitic dacite	Adakitic dacite
$^{87}Sr/^{86}Sr$	0·706676	0·706639	0·706645	0·706595	0·706655	0·707995	0·708655	0·712125
2σ, 10^{-6}	4	4	4	4	4	7	7	10
$^{143}Nd/^{144}Nd$	0·512293	0·512289	0·512313	0·512330	0·512285	0·512104	0·512102	0·511590
2σ, 10^{-6}	3	4	3	3	3	4	3	1
$^{87}Rb/^{86}Sr$	0·216	0·216	0·211	0·242	0·221	0·242	0·361	0·353
$^{147}Sm/^{144}Nd$	0·1240	0·1199	0·1252	0·1233	0·1281	0·1050	0·1088	0·0930
$(^{87}Sr/^{86}Sr)_i$	0·706290	0·706253	0·706267	0·706161	0·706260	0·707561	0·708008	0·711493
$(^{143}Nd/^{144}Nd)_i$	0·512191	0·512190	0·512210	0·512228	0·512179	0·512018	0·512012	0·511513
$\varepsilon_{Nd}(t)$	–5·56	–5·57	–5·19	–4·83	–5·78	–8·94	–9·04	–18·78
T_{DM} (Ga)	1·45	1·40	1·44	1·38	1·54	1·46	1·52	1·96
T_{DM}^2 (Ga)	1·19	1·19	1·16	1·14	1·20	1·42	1·43	2·10

$^{87}Rb/^{86}Sr$ and $^{147}Sm/^{144}Nd$ ratios are calculated using Rb, Sr, Sm and Nd contents by ICP-MS and measured $^{87}Sr/^{86}Sr$ and $^{143}Nd/^{144}Nd$ ratios by MC-ICP-MS; $^{147}Sm/^{144}Nd$ and $^{143}Nd/^{144}Nd$ ratios used in calculation of initial isotopic ratios, model ages (T_{DM}) and two-stage model ages (T_{DM}^2) are 0·1967 and 0·512638 for CHUR, and 0·2137 and 0·51315 for depleted mantle (DM), respectively; $^{87}Rb/^{86}Sr$ and $^{87}Sr/^{86}Sr$ are 0·0827 and 0·7045 for CHUR; initial isotopic ratios are calculated at 122 Ma for the lavas.

Shimadzu 1600 electron microprobe at University of Science and Technology of China (USTC) and a JEOL JXA-8230 electron microprobe at the Guangzhou Institute of Geochemistry, Chinese Academy of Sciences (GIGCAS). The accelerating voltage was 15 kV with a beam current of 20 nA and a beam diameter of 1–2 μm. The peak counting times are 30 s for Ca and Ni in olivine, 7 s for Na and K, and 10 s for the rest of the elements. Typical analytical uncertainties range from 1 to 5%, relative, except for Na, which may be up to 10%.

Major-element compositions of whole-rocks were measured by X-ray fluorescence spectrometry (XRF) using a Shimadzu XRF-1800 sequential XRF system with a voltage of 40 kV and a current of 70 mA at the

Table 3. Zircon U–Pb data for the Guiyunhua dacite (SHY-16) in the Liaodong Peninsula

Spot no.	Measured U–Pb ratios						Calculated U–Pb ages (Ma)					
	$^{207}Pb/^{206}Pb$	1σ	$^{207}Pb/^{235}U$	1σ	$^{206}Pb/^{238}U$	1σ	$^{207}Pb/^{206}Pb$	1σ	$^{207}Pb/^{235}U$	1σ	$^{206}Pb/^{238}U$	1σ
1	0·0551	0·0040	0·198	0·014	0·0265	0·0006	417	156	183	12	168	3
2	0·0875	0·0082	0·219	0·019	0·0190	0·0006	1370	156	201	15	121	4
3	0·1148	0·0089	0·304	0·028	0·0195	0·0007	1876	157	269	22	124	4
4	0·1406	0·0190	0·365	0·047	0·0188	0·0008	2234	245	316	35	120	5
5	0·1066	0·0152	0·281	0·038	0·0191	0·0008	1741	276	251	30	122	5
6	0·1140	0·0132	0·267	0·026	0·0184	0·0006	1864	174	240	21	117	3
7	0·1051	0·0141	0·269	0·035	0·0186	0·0007	1716	261	242	28	119	4
8	0·1248	0·0122	1·018	0·096	0·0592	0·0014	2026	179	713	48	371	8
9	0·0625	0·0048	0·155	0·011	0·0185	0·0004	691	144	146	9	118	2
10	0·0953	0·0127	0·256	0·033	0·0195	0·0008	1534	264	231	26	124	5
11	0·0832	0·0122	0·227	0·032	0·0198	0·0007	1273	304	207	27	126	5
12	0·0904	0·0092	0·228	0·018	0·0197	0·0007	1435	144	209	15	125	4
13	0·0717	0·0105	0·191	0·027	0·0193	0·0007	977	317	178	23	123	4
14	0·0946	0·0151	0·240	0·037	0·0184	0·0007	1519	321	218	30	117	4
15	0·0844	0·0128	0·212	0·031	0·0182	0·0008	1302	315	195	26	116	5
16	0·1076	0·0109	0·268	0·022	0·0195	0·0007	1760	138	241	17	124	4
17	0·1065	0·0118	0·242	0·024	0·0192	0·0007	1741	173	220	19	123	4
18	0·0872	0·0080	0·230	0·016	0·0207	0·0008	1366	119	210	13	132	5
19	0·0979	0·0133	0·254	0·033	0·0188	0·0007	1585	268	230	27	120	5
20r	0·0804	0·0111	0·226	0·030	0·0204	0·0007	1208	288	207	25	130	4
20c	0·1062	0·0039	4·023	0·146	0·2675	0·0045	1734	60	1639	30	1528	23
21	0·0810	0·0113	0·205	0·027	0·0183	0·0008	1222	292	189	23	117	5
22	0·0909	0·0092	0·241	0·023	0·0202	0·0006	1445	177	219	19	129	4

Table 4. Hf isotopic data for zircons from the Guiyunhua dacite (SHY-16) in the Liaodong Peninsula

Spot no.	$^{176}Hf/^{177}Hf$	1σ	$^{176}Lu/^{177}Hf$	$^{176}Yb/^{177}Hf$	$^{176}Hf/^{177}Hf_i$	$\varepsilon_{Hf}(t)$	1σ	T_{DM} (Ga)	T_{crust} (Ga)
2	0·282087	0·000008	0·000680	0·021298	0·282085	–21·6	0·3	1·63	2·54
3	0·282086	0·000008	0·000201	0·006750	0·282086	–21·6	0·3	1·61	2·54
4	0·282097	0·000009	0·000813	0·025400	0·282095	–21·3	0·3	1·62	2·52
5	0·282084	0·000006	0·000559	0·016723	0·282083	–21·7	0·2	1·63	2·54
6	0·282069	0·000008	0·000417	0·012313	0·282068	–22·2	0·3	1·64	2·58
7	0·282054	0·000010	0·000496	0·014566	0·282053	–22·8	0·3	1·67	2·61
9	0·282092	0·000010	0·001544	0·048055	0·282088	–21·5	0·3	1·66	2·53
10	0·282081	0·000007	0·000363	0·010659	0·282080	–21·8	0·3	1·62	2·55
11	0·282070	0·000009	0·000639	0·019186	0·282068	–22·2	0·3	1·65	2·58
12	0·282102	0·000006	0·000420	0·012313	0·282101	–21·1	0·2	1·60	2·50
13	0·282103	0·000006	0·000625	0·019804	0·282101	–21·1	0·2	1·60	2·50
14	0·282093	0·000005	0·000422	0·012384	0·282092	–21·4	0·2	1·61	2·52
15	0·282054	0·000006	0·000667	0·020437	0·282053	–22·8	0·2	1·67	2·61
16	0·282074	0·000008	0·000494	0·014525	0·282073	–22·1	0·3	1·64	2·57
17	0·282070	0·000005	0·000399	0·011566	0·282069	–22·2	0·2	1·64	2·57

Initial isotopic ratios and $\varepsilon_{Hf}(t)$ are calculated at 122 Ma for the lavas.

Table 5. P–T estimation by different thermobarometers for early Cretaceous Guiyunhua lavas in the Liaodong Peninsula

Sample: Rock type:	SHY13 Ol-HMAs	SHY04 Cpx-HMAs	SHY15 High-Mg adakitic dacite	SHY15 High-Mg adakitic dacite	SHY15 High-Mg adakitic dacite	SHY15 High-Mg adakitic dacite
n	5	2	6	6	6	6
Thermobarometry	Cpx–melt*	Cpx–melt*	Am	Am	Am	Am
Reference	Putirka *et al.* (2003)	Putirka *et al.* (2003)	Hollister *et al.* (1987)	Johnson & Rutherford (1989)	Anderson & Smith (1995)	Ridolfi *et al.* (2010)
P (kbar)	9·2–10·9	6·6–7·5	3·1–4·8	2·5–3·7	3·6–5·0	1·4–2·2
T (°C)	1235–1250	1202–1209				836–895
H_2O (wt %)						5·0–5·7

*Compositions of melt are assumed to be those of the whole-rocks.
n, number of estimation.

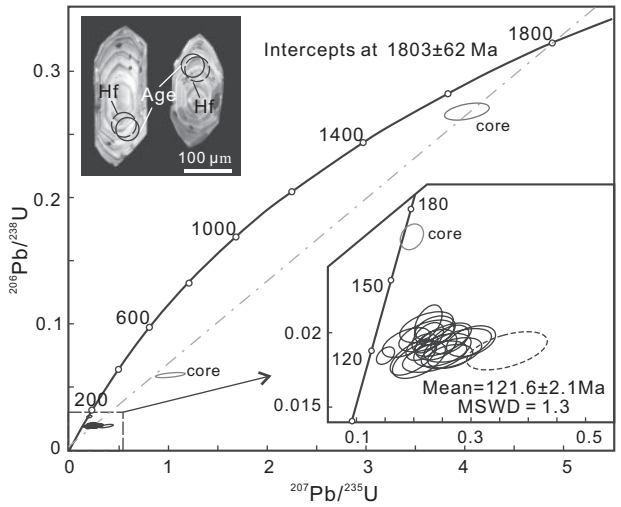

Fig. 3. U–Pb concordia diagram and representative cathodoluminescence (CL) images for zircons from Guiyunhua dacite SHY16 from the Liaodong Peninsula, North China.

China University of Geosciences, Wuhan (CUG). The measurement procedure and data quality were monitored by repeated samples and USGS standard AGV-2; the analytical uncertainties are better than 3%. Detailed sample fusion procedures and analytical precision and accuracy have been described by Ma *et al.* (2012). Trace-element concentrations of whole-rocks were determined by inductively coupled plasma mass spectrometry (ICP-MS) at GIGCAS using a Perkin–Elmer Sciex ELAN 600 system after acid digestion of the samples in high-pressure Teflon bombs, following the analytical procedures described by Liu *et al.* (1996). Analytical uncertainties are better than 5% for most trace elements and are better than 10% for others (Cr and Pb).

Sr and Nd isotopic ratios of whole-rocks were analyzed by multicollector (MC)-ICP-MS using a Micromass Isoprobe system after digestion in Teflon bombs with a mixture of concentrated HF, HNO_3 and $HClO_4$ at GIGCAS. Detailed sample digestion and separation procedure, and analytical techniques follow those of Wei *et al.* (2002) and Li *et al.* (2004). The measured $^{87}Sr/^{86}Sr$ and $^{143}Nd/^{144}Nd$ ratios were normalized to $^{86}Sr/^{88}Sr = 0{\cdot}1194$ and $^{146}Nd/^{144}Nd = 0{\cdot}7219$, respectively. SRM NBS-987 yielded an average $^{87}Sr/^{86}Sr$ of $0{\cdot}710243 \pm 14$ (2σ; $n = 12$). The La Jolla standard measured during the course of analysis yielded an average $^{143}Nd/^{144}Nd$ of $0{\cdot}511847 \pm 3$ (2σ; $n = 11$), and BHVO-2 yielded $^{143}Nd/^{144}Nd$ of $0{\cdot}512979 \pm 6$ (2σ; $n = 3$). $^{87}Rb/^{86}Sr$ and $^{147}Sm/^{144}Nd$ ratios were calculated using measured $^{87}Sr/^{86}Sr$ and $^{143}Nd/^{144}Nd$ ratios by MC-ICP-MS, and Rb, Sr, Sm and Nd contents by ICP-MS. Initial isotopic ratios and $\varepsilon_{Nd}(t)$ were calculated using an age of 122 Ma for the lavas.

Cathodoluminescence (CL) images, U–Pb dating and Hf isotope analyses of zircon were conducted at CUG. CL images of zircon were obtained prior to analysis, using a JXA-8100 electron microprobe, to characterize the internal structures and to select suitable sites for U–Pb dating and Hf isotope analyses. *In situ* U–Pb isotope analyses of zircon were conducted by LA-ICP-MS with a beam diameter of 32 μm and zircon 91500 as external standard. Zircon Lu–Hf isotope analyses were conducted using a Neptune Plus MC-ICP-MS system in combination with a Geolas 2005 excimer ArF laser ablation (LA) system, using a beam diameter of 44 μm. Detailed operating conditions and data reduction for zircon U–Pb dating and Hf isotope analyses have been described by Liu *et al.* (2010) and Hu *et al.* (2012). U–Pb age data were not subjected to a common-lead correction because the common-Pb concentrations were lower than detection limits. Concordia diagrams and weighted mean calculations were made using Isoplot/Ex_ver3 (Ludwig, 2003). Calculation of initial Hf isotope ratios and model ages used the ^{176}Lu decay constant of $1{\cdot}865 \times 10^{-11}$ (Amelin & Davis, 2005). The $^{176}Hf/^{177}Hf$ and $^{176}Lu/^{177}Hf$ ratios of CHUR and depleted mantle are 0·282772 and 0·0332, and 0·28325 and 0·0384, respectively (Blichert-Toft & Albarède, 1997; Griffin *et al.*, 2000). Initial isotopic ratios and $\varepsilon_{Hf}(t)$ were calculated using an age of 122 Ma for the lavas.

RESULTS

Zircon U–Pb dating

Zircons from a dacite (SHY16) were used to constrain the eruption age of the Guiyunhua volcanic rocks. The zircon grains are euhedral, 100–350 μm long and have length/width ratios of 2:1 to 4:1. Most of them show clear oscillatory zoning in CL images (Fig. 3), typical of magmatic zircons. Inherited cores with older ages were also observed in some grains. The magmatic zircon grains yield apparent $^{206}Pb/^{238}U$ ages ranging from 116 to 132 Ma, with a weighted mean $^{206}Pb/^{238}U$ age of 122 ± 2 Ma (MSWD = 1·3), which is interpreted as the crystallization age of dacite SHY16. Similar early Cretaceous ages (106–132 Ma) have also been reported for the Guiyunhua lavas in different supra-detachment basins in the MCC in the Liaodong Peninsula (Liu *et al.*, 2011; Shen *et al.*, 2011; Fig. 1b).

Mineral chemistry

Olivine

Olivine phenocrysts in the Guiyunhua Ol-HMAs are magnesian with Fo contents [$Fo = 100 \times Mg/(Mg + Fe)$] varying from 84·4 to 90·8 (Fig. 4a and b). Calculated Mg–Fe partition coefficients between the cores of the most forsteritic phenocrysts ($Fo > 90$) and whole-rocks range from 0·28 to 0·34 (Fig. 5a), consistent with experimental values between olivine and basaltic melt of $0{\cdot}30 \pm 0{\cdot}03$ (Roeder & Emslie, 1970). Their CaO contents (0·08 wt %) are higher than those of olivine from mantle xenoliths in the NCC (Fig. 5b), which suggests that they precipitated from magmas, rather than being mantle xenocrysts. The NiO contents of olivine in the Ol-HMAs decrease with decreasing Fo content (Fig. 5c), which

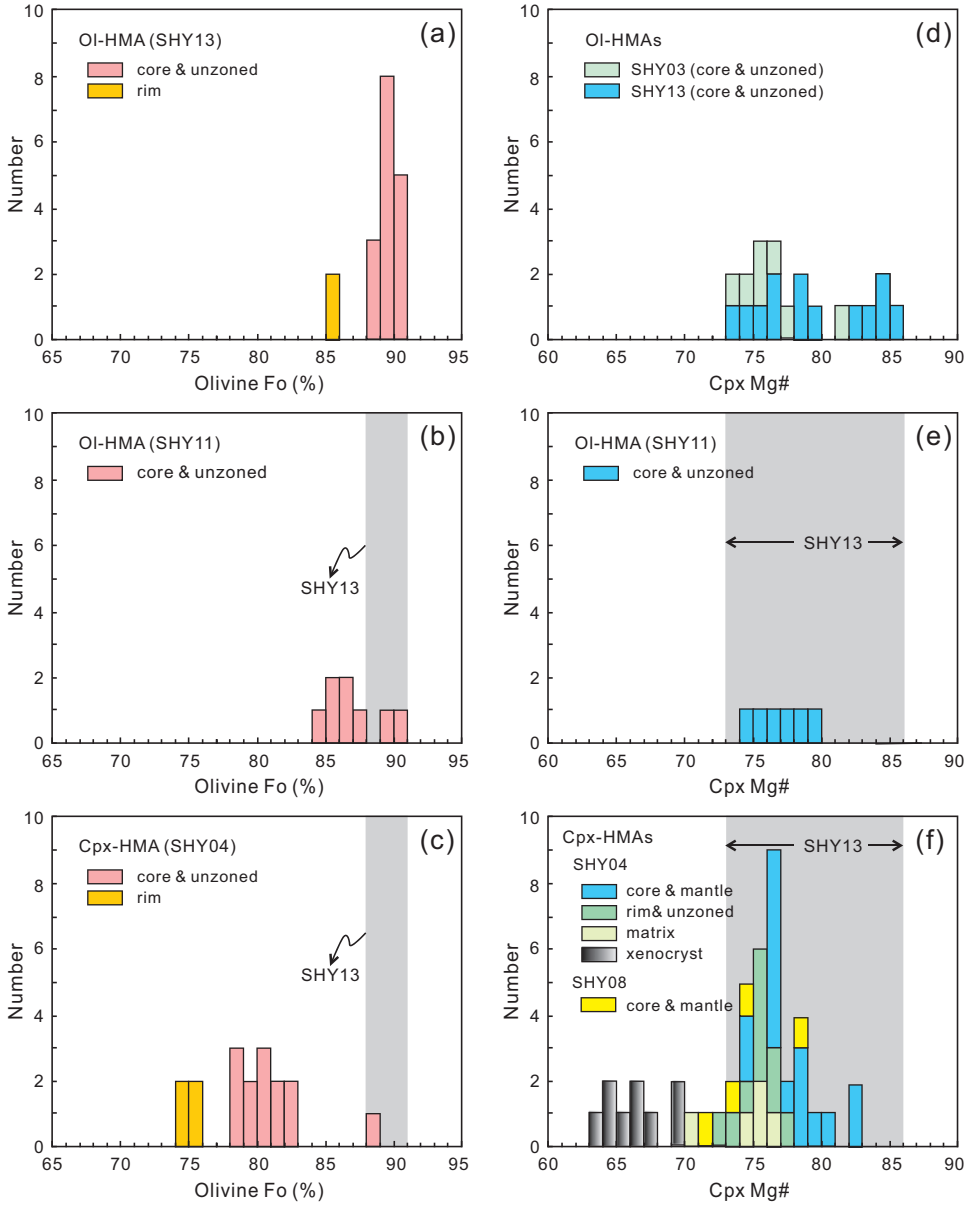

Fig. 4. Histograms of Fo content of olivine phenocrysts (a–c) and Mg-numbers of clinopyroxene (d–f) in early Cretaceous Guiyunhua HMAs of the Liaodong Peninsula. For comparison, the compositions of phenocrysts from Ol-HMA SHY13 are also shown in (b, c) and (e, f).

also distinguishes them from the array defined by mantle xenoliths (Sato, 1977).

Olivine phenocrysts in the Guiyunhua Cpx-HMAs have lower Fo contents (74·1–88·3) than those in the Ol-HMAs (Fig. 4c). One olivine falls within the equilibrium field, whereas the remaining grains fall significantly below the equilibrium field in an Fe–Mg equilibrium diagram (Fig. 5a), suggesting that the analyzed olivines are not equilibrium phenocrysts. They have higher CaO and lower NiO contents than those in the Ol-HMAs (Fig. 5b and c), which also suggests that they are late-crystallizing grains.

Clinopyroxene

Clinopyroxenes in the Guiyunhua Ol-HMAs are mainly augite and subordinate diopside (Supplementary Data Fig. S1 in Electronic Appendix 4; supplementary data are available for downloading at http://www.petrology.oxfordjournals.org), with Mg# values ranging from 73·1 to 85·6 (Fig. 4d and e), and low Al_2O_3 (<4·5 wt %) and Na_2O (<0·6 wt %). Clinopyroxene phenocrysts in the Ol-HMAs are euhedral and mostly homogeneous. Some crystals exhibit weak compositional zoning with cores having slightly lower Mg# than the rims. Such textural and chemical variation probably reflects

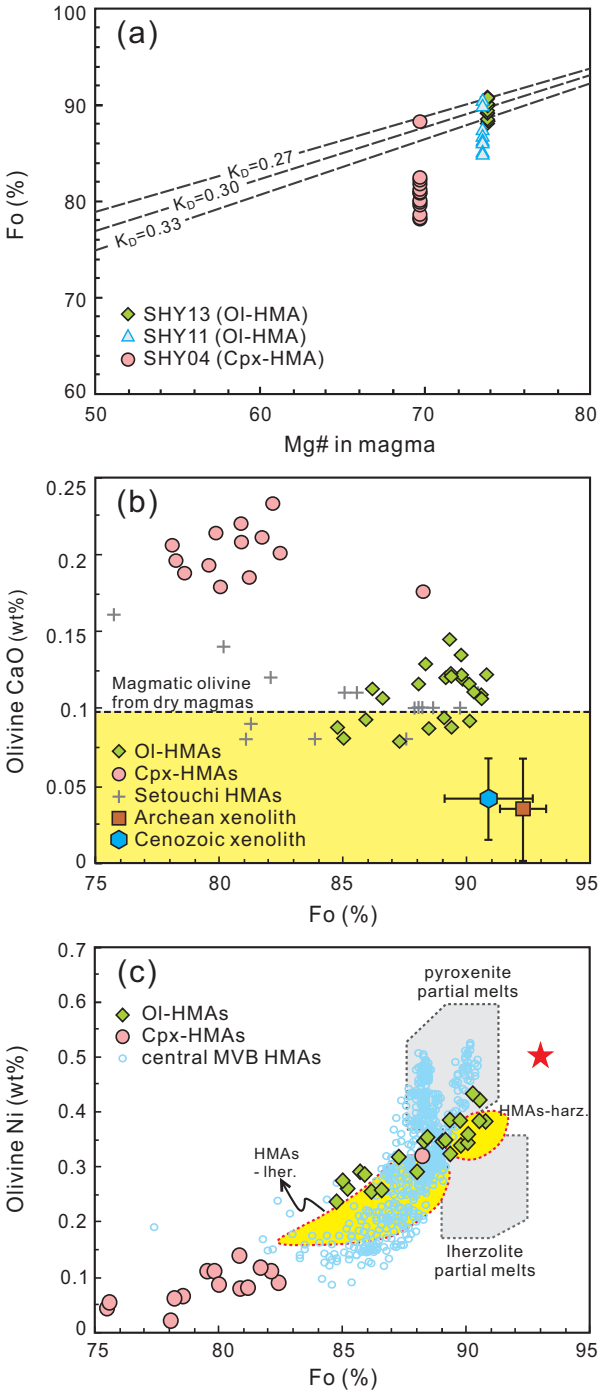

Fig. 5. (a) Fe/Mg equilibrium between olivine cores (Fo content) and whole-rock compositions (Mg#) in early Cretaceous Guiyunhua HMAs, where the Mg# of the whole-rocks was calculated assuming 10% of total Fe as Fe^{3+}. The Fe/Mg exchange partition coefficient between olivine and basaltic liquid is taken as 0·30 ± 0·03 (Roeder & Emslie, 1970). (b) Variation of CaO and (c) Ni contents vs Fo content of olivine cores from early Cretaceous Guiyunhua HMAs. The dashed line in (b) separates magmatic and xenocrystic olivine in dry mafic magmas on the basis of CaO content (Foley *et al.*, 2013). Compositions of olivine in Archean peridotite xenoliths from Ordovician kimberlites and those in lherzolite xenoliths from Cenozoic alkali basalts in the NCC are from Gao *et al.* (2008). Compositions of olivine in HMAs from the Setouchi volcanic belt, Japan (Setouchi HMAs) in (b) are from Tatsumi *et al.* (2006). Compositions of olivine from anhydrous melts in equilibrium with mantle lherzolite and pyroxenite are from Straub *et al.* (2011). Fields of olivine from Setouchi HMAs in equilibrium with mantle lherzolite (HMAs-lher.) and harzburgite (HMAs-harz.) are modified from Tatsumi *et al.* (2003). Olivine phenocrysts in calc-alkaline basaltic andesites and andesites from the central Mexican Volcanic Belt (central MVB HMAs) are after Straub *et al.* (2008). Red star in (c) indicates olivine in peridotite that has undergone 70% serial depletion (Straub *et al.*, 2008).

rapid crystallization during magma ascent (Guo *et al.*, 2007).

Clinopyroxenes in the Guiyunhua Cpx-HMAs are mainly diopside and subordinate augite (Supplementary Data Fig. S1 in Electronic Appendix 4), with variable Mg# (63·7–82·7; Fig. 4f) and low Na_2O (<0·8 wt %). These clinopyroxene phenocrysts have more complex textural and chemical variation than those from the Ol-HMAs. Green-cored, unzoned, normally zoned and weakly reverse zoned clinopyroxene all are found in the Cpx-HMAs (Supplementary Data Fig. S2 in Electronic Appendix 4). The green-cored Cpx (<3%) has a resorbed green core surrounded by a colorless mantle and thin rim (Fig. 2d). This type of clinopyroxene has a low-Mg# (<70) core and shows an abrupt increase in Mg# to >75 in the mantle (Supplementary Data Fig. S2 in Electronic Appendix 4). Some of them are partially (core) or completely pseudomorphed by a vermicular aggregate of fine-grained pyroxene, magnetite, plagioclase, olivine and albite (Supplementary Data Fig. S3 in Electronic Appendix 4). Compositions of the green, resorbed and low-Mg# (<70) cores are very similar to those of clinopyroxenes from the lower crust of the NCC (Supplementary Data Fig. S4 in Electronic Appendix 4), and the morphologies, structure and composition of green-cored Cpx probably reflect overgrowth around lower crustal xenocrystic clinopyroxene. The magmatic clinopyroxene phenocrysts from the Cpx-HMAs have lower Mg# (72·9–82·7; Fig. 4f) and higher Al_2O_3 (3·3–8·5 wt %) than those from the Ol-HMA.

Clinopyroxene phenocrysts in the Guiyunhua dacites are subhedral to euhedral and rimmed by amphibole. They are diopside and augite (Fig. S1 in Electronic Appendix 4) with compositions similar to the non-zoned Cpx and the rim of zoned Cpx from the Cpx-HMAs.

Amphibole, plagioclase and magnetite

Amphibole phenocrysts in dacites are euhedral and homogeneous and are classified as magnesio-hastingsite of the calcic-amphibole group according to the nomenclature of Leake *et al.* (1997). Their cores have MgO, FeO and Al_2O_3 of 15·0–16·3 wt %, 10·2–12·1 wt % and 8·4–9·9 wt %, respectively.

Plagioclase is present in the groundmass and the reacted cores of green-cored Cpx in the Guiyunhua HMAs. They are andesine with end-member compositions of $Ab_{28·5–44·5}An_{58·1–70·5}Or_{1·0–2·5}$. Plagioclase phenocrysts in the Guiyunhua dacite (SHY15) are

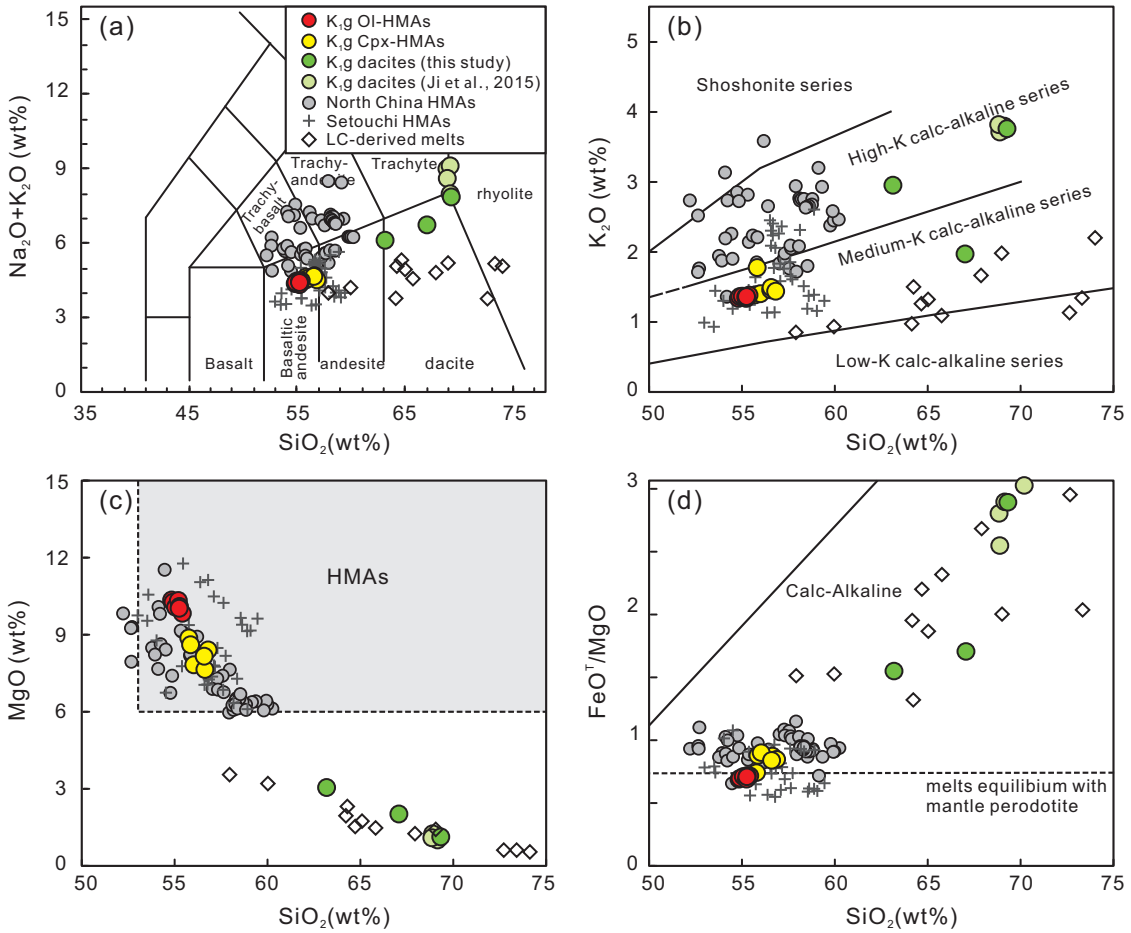

Fig. 6. Variation of (a) $Na_2O + K_2O$, (b) K_2O, (c) MgO and (d) FeO^T/MgO vs SiO_2 for early Cretaceous Guiyunhua volcanic rocks of the Liaodong Peninsula. Early Cretaceous Guiyunhua trachy-dacites in the Pulandian basin (Fig. 1) are from Ji *et al.* (2015). Data for early Cretaceous high-Mg andesites and diorites in North China (North China HMAs) are from Zhang *et al.* (2003), Wang *et al.* (2006), Yang & Li (2008), Xu *et al.* (2008) and Chen *et al.* (2013); HMAs in the Setouchi volcanic belt, Japan, are from Tatsumi & Ishizaka (1982), Shimoda *et al.* (1998) and Tatsumi *et al.* (2003); data for experimental melts of mafic lower crust at 1–1·5 GPa (LC-derived melts) are from Qian & Hermann (2013). K_1g represents Early Cretaceous Guiyunhua volcanic rocks (LBGMR, 1989).

labradorite and andesine with end-member compositions of $Ab_{37·6–53·2}An_{43·0–51·1}Or_{1·7–9·0}$.

Fe–Ti oxides are rare in the Ol-HMAs and occur only in the groundmass. However, more magnetite occurs as phenocrysts and as a groundmass mineral in the Cpx-HMAs (Supplementary Data Fig. S3 in Electronic Appendix 4). They are titanomagnetite with a wide range of TiO_2, from ~14·5 wt % in magnetite included in the green-cored Cpx to ~17·7 wt % in the groundmass phase.

Whole-rock chemistry

The Guiyunhua high-Mg volcanic rocks encompass medium-K basaltic andesites and medium-K to high-K dacites (Fig. 6a and b). Major element compositions are discussed in terms of weight per cent, normalized to 100% on a volatile-free basis.

High-Mg andesites

The basaltic andesites have high SiO_2 (54·8–56·8 wt %), high MgO (7·6–10·4 wt %; Fig. 6c), low FeO^T/MgO (<1; Fig. 6d) and high Mg# (67–72), corresponding to the geochemical characteristics of HMAs (Crawford *et al.*, 1989; Le Bas, 2000; Tatsumi, 2006). They also exhibit moderate CaO (7·1–8·0 wt %) and Al_2O_3 (13·7–14·9 wt %), low TiO_2 (<0·8 wt %) and P_2O_5 (<0·2 wt %), and high Ni (234–310 ppm) and Cr (524–612 ppm) (Fig. 7), and thus are similar to the Neogene HMAs in the Setouchi volcanic belt of Japan (Tatsumi, 2006).

The chondrite-normalized REE patterns (Fig. 8a) of the HMA show enrichment of LREE over heavy REE (HREE) with negligible Eu anomalies [$\delta_{Eu} = 0·9–1·0$, where $\delta_{Eu} = 2 \times Eu_N/(Sm_N + Gd_N)$] and fractionation of middle REE (MREE) versus HREE ($Sm_N/Yb_N \leq 3·0$). They are enriched in LREE, LILE (Rb, Ba and Th) and Pb, with negative anomalies in high field strength elements (HFSE; Nb, Ta and Ti) in the primitive mantle-normalized trace element patterns (Fig. 8b).

Adakitic dacites

The dacites have high SiO_2 (>63 wt %), Na_2O (>3·2 wt %) and K_2O (>2·0 wt %). Compared with the coexisting

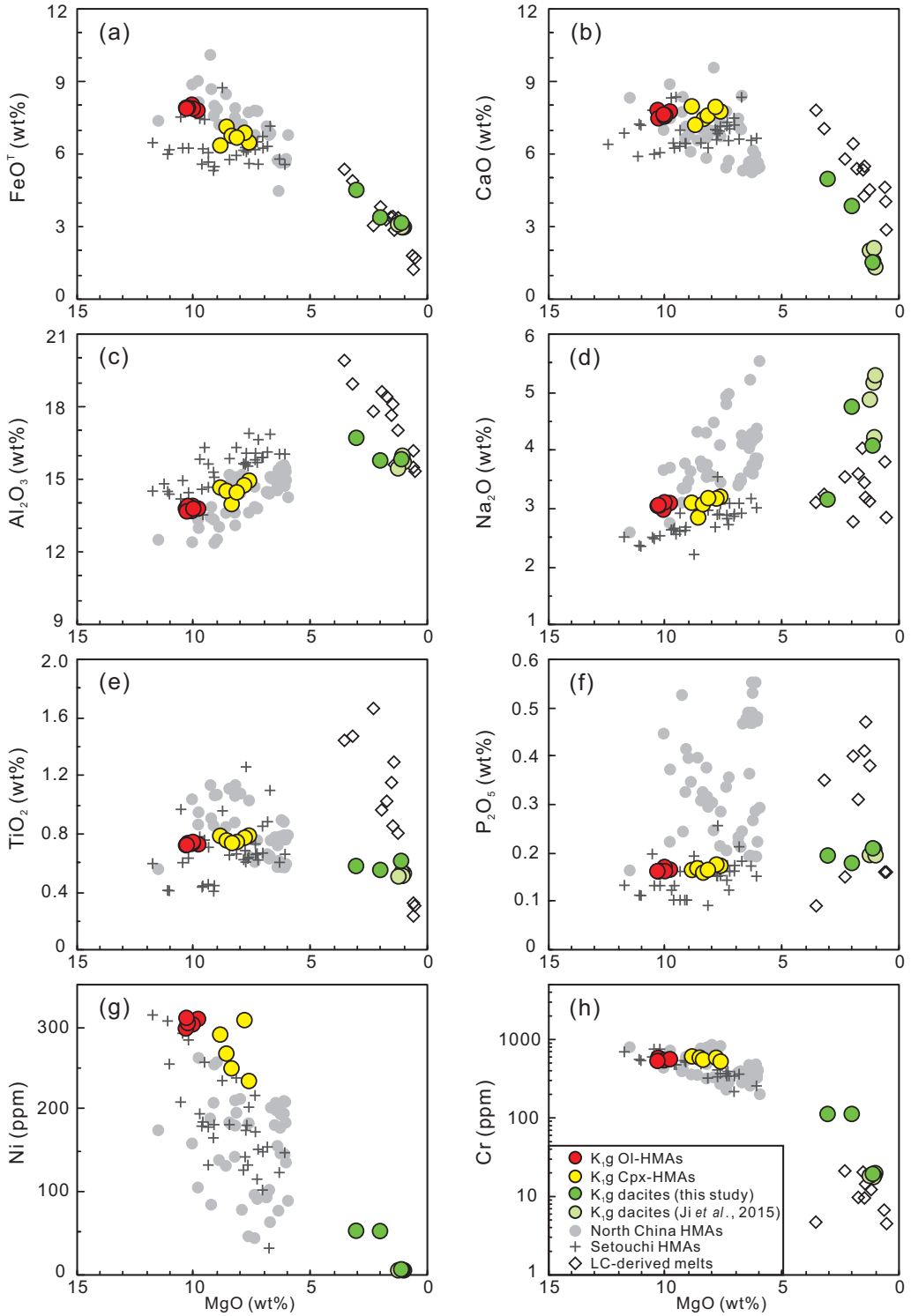

Fig. 7. Variation of (a) FeO^T, (b) CaO, (c) Al_2O_3, (d) Na_2O, (e) TiO_2, (f) P_2O_5, (g) Ni and (h) Cr vs MgO for early Cretaceous Guiyunhua volcanic rocks in the Liaodong Peninsula. The whole-rock compositions have been recalculated to 100% on an anhydrous basis. Data sources are as in Fig. 6. The discrepancy between Na_2O, TiO_2 and CaO contents in the dacites and those for experimental lower crustal derived melts may be attributed to the different compositions of the starting materials of the experiments and the mafic lower crust of the NCC. K_1g represents Early Cretaceous Guiyunhua volcanic rocks (LBGMR, 1989).

HMAs, these dacites have lower MgO, FeO, CaO, Ni and Cr, and higher Al_2O_3 (Fig. 7). They are characterized by adakitic trace element signatures (Ma *et al.*, 2015) with high Sr ($\geq$485 ppm) and LREE, low Y ($\leq$14 ppm) and HREE (Yb $\leq$ 1·2 ppm), a lack of obvious Eu anomalies (δ_{Eu} = 0·9–1·0; Fig. 8a), and high Sr/Y ($\geq$39; Fig. 9a); in all these features they are broadly similar to both modern adakites and Archean TTG suites (Defant & Drummond,

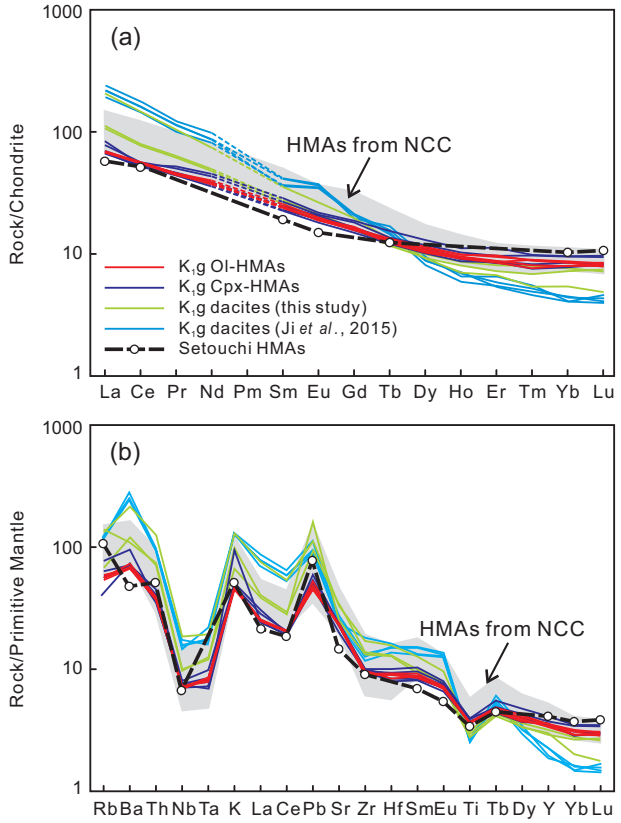

Fig. 8. Chondrite-normalized REE patterns (a) and primitive mantle-normalized trace-element patterns (b) for early Cretaceous Guiyunhua volcanic rocks in the Liaodong Peninsula. Normalizing values are from McDonough & Sun (1995). K_1g represents Early Cretaceous Guiyunhua volcanic rocks (LBGMR, 1989).

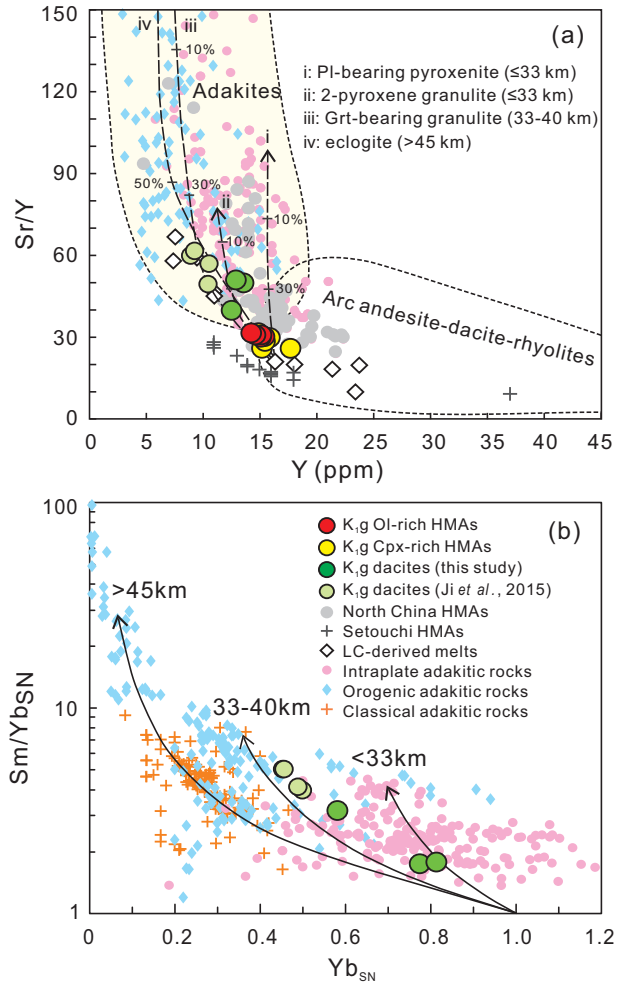

Fig. 9. Variation of Sr/Y vs Y (a) and $(Sm/Yb)_{SN}$ vs Yb_{SN} (b) for early Cretaceous Guiyunhua volcanic rocks from the Liaodong Peninsula. Fields of adakites and typical arc andesite–dacite–rhyolites in (a) are modified from Defant & Drummond (1990). Partial-melting curves in (a) are calculated for batch melting of the mafic lower crust of the NCC (Ma *et al.*, 2015). The curves in (b) represent models for the partial melting of mafic rocks at different pressures (Ma *et al.*, 2015). Data for intraplate, orogenic and classical adakitic rocks are compiled from Ma *et al.* (2015). Subscript SN denotes source-normalized data, where the compositions of the assumed sources are MORB with Yb = 3 ppm and Sm/Yb = 1·08 for classical adakites and mafic lower continental crust with Yb = 1·5 ppm and Sm/Yb = 1·87 for continental (intraplate and orogenic) adakitic rocks (Ma *et al.*, 2015). K_1g represents Early Cretaceous Guiyunhua volcanic rocks (LBGMR, 1989).

1990; Martin *et al.*, 2005) and to experimental melts of mafic lower crust at pressures of 1–1·25 GPa (Qian & Hermann, 2013). They are enriched in LREE, LILE (e.g. Rb, Ba and Th) and Pb, with negative anomalies in HFSE (Nb, Ta and Ti) in primitive mantle-normalized trace element patterns (Fig. 8b). Dacite SHY16, which has the highest SiO_2 (69·3 wt %), as well as Guiyunhua dacite–trachydacite from the nearby Pulandian basin (Fig. 1; Ji *et al.*, 2015) are defined as low-Mg adakitic dacites in this study, based on their low MgO (<1·2 wt %), Mg# (<41), Ni (<7 ppm) and Cr (<20 ppm). The remaining two dacite samples (SHY14 and SHY15), defined as high-Mg adakitic dacites in this study, have moderate MgO (2·0–3·1 wt %) but higher Mg# (>51), Ni (~53 ppm) and Cr (~112 ppm) than the low-Mg adakitic dacites and experimental melts equilibrated with basaltic rocks at 1–4 GPa (Rapp *et al.*, 1999; Qian & Hermann, 2013). These high-Mg dacites have lower LREE and LILE and higher HREE contents than the low-Mg dacites and plot between HMA and low-Mg dacites in chondrite-normalized REE (Fig. 8a) and primitive mantle-normalized trace element (Fig. 8b) patterns.

Whole-rock Sr–Nd isotope compositions

Initial $^{87}Sr/^{86}Sr$ ratios and $\varepsilon_{Nd}(t)$ values have been calculated at 122 Ma, corresponding to the zircon U–Pb age of the adakitic dacite, and are shown in a plot of $\varepsilon_{Nd}(t)$ vs $(^{87}Sr/^{86}Sr)_i$ (Fig. 10a). The Sr–Nd isotopic compositions of the Guiyunhua HMAs (both OI- and Cpx-HMAs) are homogeneous with $(^{87}Sr/^{86}Sr)_i$ of 0·7062–0·7063 and negative $\varepsilon_{Nd}(t)$ values of –5·8 to –4·9 (Table 2), comparable with the Nd isotopic composition of Mesozoic subcontinental lithospheric mantle (SCLM) beneath the NCC (Fig. 10a). In contrast, the adakitic dacites have

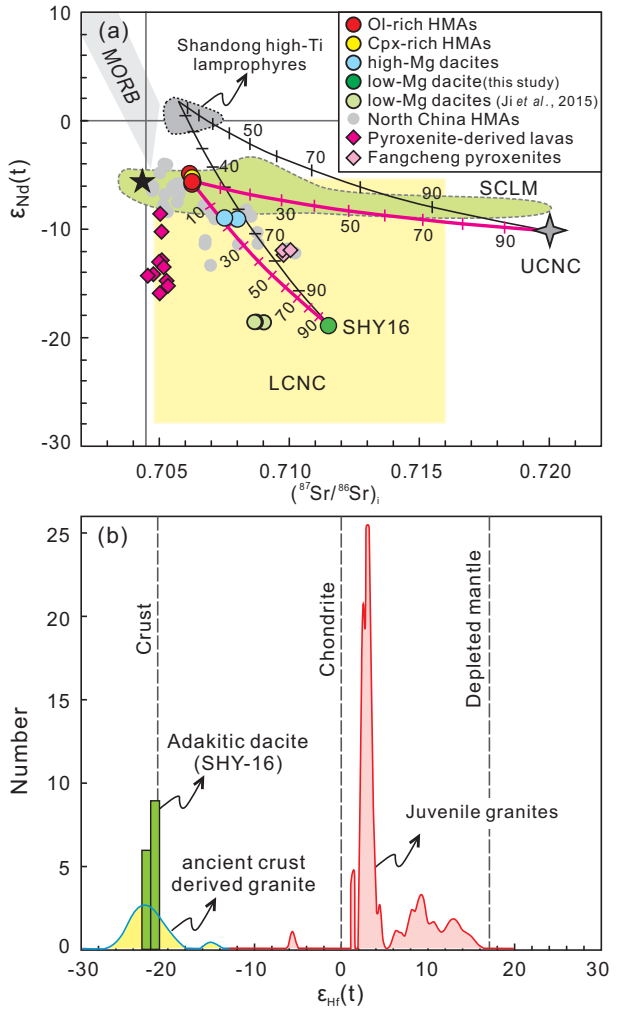

Fig. 10. Whole-rock Sr–Nd (a) and zircon Hf (b) isotopic compositions of early Cretaceous Guiyunhua volcanic rocks in the Liaodong Peninsula. The numbers on the mixing curves in (a) indicate the percentages of lower crustal derived melts (SHY16) and upper crust (UCNC; Jahn *et al.*, 1999). Early Cretaceous asthenospheric mantle-derived high-Ti lamprophyres in Shandong Province (Shandong high-Ti lamprophyres) are from Ma *et al.* (2014). Pyroxenites in early Cretaceous Fangcheng basalts from Shandong Province (Fangcheng pyroxenites) are from Zhang *et al.* (2008). Early Cretaceous mafic lavas that have been proposed to be derived from a pyroxenitic mantle source in the Liaodong Peninsula (pyroxenite-derived lavas) are from Pang *et al.* (2015). Field of Sr–Nd isotopes of MORB in (a) is after http://www.earthchem.org/petdb. Field of lower crust of the NCC (LCNC) is modified from Jiang *et al.* (2013). Subcontinental lithospheric mantle (SCLM) beneath the NCC is represented by peridotite xenoliths and perovskite from Paleozoic kimberlites (Zheng & Lu, 1999; Zhang & Yang, 2007; Zhang *et al.*, 2008; Yang *et al.*, 2009). Early Cretaceous granites derived from ancient lower crust (Gudaoling monzogranite) and those with contributions of juvenile crust in (b) are from Yang *et al.* (2007*b*) and Yang *et al.* (2008), respectively. Initial Sr isotopic ratios, $\varepsilon_{Nd}(t)$ and $\varepsilon_{Hf}(t)$ are calculated at 122 Ma. Black star in (a) indicates the mantle end-member used in the mixing calculation of Fig. 14.

distinctly different Sr and Nd isotopic compositions, with a wide range of initial $^{87}Sr/^{86}Sr$ (0·7076–0·7115) and $\varepsilon_{Nd}(t)$ (–18·9 to –8·9), similar to that of the lower crust beneath the NCC (Jiang *et al.*, 2013). The high-Mg adakitic lavas have less radiogenic initial Sr and more radiogenic Nd isotope compositions than the low-Mg group and plot on a binary mixing line between the HMAs and the low-Mg dacite SHY16.

Zircon Hf isotope compositions

Magmatic zircons from adakitic dacite SHY16 have homogeneous isotopic compositions with initial $^{176}Hf/^{177}Hf$ ratios from 0·282053 to 0·282101, $\varepsilon_{Hf}(t)$ values from –21·1 to –22·8, depleted mantle Hf model ages (T_{DM}) from 1·6 to 1·7 Ga and crustal model ages (T_{DM}^{C}) ranging from 2·5 to 2·6 Ga. The Hf-isotope compositions are very similar to those of zircon in contemporary granites derived from the ancient lower crust (Yang *et al.*, 2007*b*), rather than those of zircon in contemporary granites in the Liaodong Peninsula, which indicate contributions from juvenile crust (Yang *et al.*, 2008) (Fig. 10b).

DISCUSSION

Crystallization pressure and temperature

High-Mg andesites (HMAs)

Clinopyroxene–liquid thermobarometers are often used to determine the temperature and pressure at which these two phases were last in equilibrium (Putirka, 2008). These thermobarometers require knowledge of whether the magma is anhydrous or hydrous. The Guiyunhua HMAs are considered as H_2O-rich magmas, on the basis of the following observations.

1. The absence of plagioclase phenocrysts in the HMA indicates that the magmas may contain abundant water, as crystallization of plagioclase is suppressed in H_2O-rich magmas (Gaetani *et al.*, 1993; Grove *et al.*, 2012).
2. Although olivine in the HMA has CaO contents higher than those from mantle xenoliths in the NCC, high-Mg and low-Ca (CaO < 0·1 wt %) phenocrysts are also present (Fig. 5b). In this respect they are similar to olivine crystals from subduction-related hydrous magmas (e.g. Kamenetsky *et al.*, 2006). The presence of water in magmas will reduce the partitioning of Ca into olivine, because the activity of Ca is suppressed by the strong bonding of hydrous species to Ca-complexes (Li *et al.*, 2012; Guo *et al.*, 2013). Therefore, low-Ca (CaO < 0·1 wt %) magmatic olivine may precipitate from a hydrous melt.
3. Magmatic clinopyroxenes from the HMA have relatively high Wo and low CaTs + CrTs [Ca(Ar,Cr)$SiAlO_6$] components, comparable with pyroxenes that crystallize from subduction-related lavas and from melts in H_2O-saturated melting experiments (Supplementary Data Fig. S5 in Electronic Appendix 4).
4. P–T–X_{H2O} estimations for Guiyunhua primary HMA magma generation suggest a hydrous melting of mantle peridotite [see 'Melting conditions (P–T–X_{H2O})', below].

Following these considerations, the crystallization pressure and temperature of the HMA were estimated using the clinopyroxene–liquid thermobarometers for hydrous systems (Putirka *et al.*, 2003). The liquid compositions used in the calculation are the whole-rock compositions without correction for the proportion of phenocrysts, because the Guiyunhua HMAs (SHY04 and SHY13) are phenocryst-poor (<7%), and small volumes of crystals do not significantly change the chemical composition of the melt (Mordick & Glazner, 2006). Tests for equilibrium between clinopyroxene and a nominal coexisting liquid can be made by comparing observed and predicted values for the Fe–Mg exchange partition coefficient [$K_D^{Fe-Mg} = (Mg^{liq}Fe^{mineral})/(Mg^{mineral}Fe^{liq})$] (Putirka, 2008). The K_D^{Fe-Mg} between clinopyroxene and basaltic melt is less well constrained than that for olivine and melt because it is *P–T* sensitive and there is some ferric iron in clinopyroxene and in the melt (Putirka *et al.*, 2003; Müller *et al.*, 2013). Values for K_D^{Fe-Mg} (Cpx–melt) from experiments at 850–1875°C and 0·001–110 kbar are distributed normally within the range 0·105–0·488 (Putirka *et al.*, 2003). Consequently, Cpx phenocrysts with calculated K_D^{Fe-Mg} beyond this range were eliminated from the *P–T* estimation. Results show that the Guiyunhua HMAs reflect high crystallization pressures (>9 and >6·5 kbar for the Ol-HMA and the Cpx-HMA, respectively) and temperatures (1235–1250°C and 1202–1209°C for the Ol-HMA and the Cpx-HMA, respectively) (Table 5).

Adakitic dacites

The crystallization pressure of the Guiyunhua adakitic dacite (SHY15) was estimated using the Al-in-hornblende thermobarometer (Table 5). The crystallization temperature and H_2O content of the melt were estimated using the thermobarometric and hygrometric formulations proposed by Ridolfi *et al.* (2010). Results show that the Guiyunhua adakitic dacites are hydrous ($H_2O \geq 5$ wt %) and record lower crystallization temperatures (836–895°C) and shallower crystallization depths (1·4–5·0 kbar) than the HMA.

Petrogenesis of the Guiyunhua HMA

A primary magma is defined as a melt that has not been modified chemically since it last equilibrated with its source region. The early Cretaceous Guiyunhua Ol-HMAs are phenocryst-poor with Mg# greater than 71 and FeO^T/MgO ratios lower than 0·72 (Fig. 6d). Their olivine phenocrysts are high-Fo (up to 90·8; Fig. 4a and b), Ni-rich (Fig. 5c) and in equilibrium with the melt composition. Hence, the Guiyunhua Ol-HMAs can be taken as primary or near-primary magmas that last equilibrated with mantle ultramafic rocks (peridotite or pyroxenite). As such, these Ol-HMAs are used to constrain the source lithology and melting conditions of the intraplate HMA magmas in the Liaodong Peninsula.

Source: peridotite vs pyroxenite?

A primary magma could have equilibrated with either a peridotite or pyroxenite residue within the mantle. Partial melts of pyroxenite (olivine-free source) have relatively low MgO and high Ni concentrations, and the early crystallizing olivine from such melts has correspondingly high Ni concentrations owing to high olivine/melt D_{Ni} (Sobolev *et al.*, 2005; Herzberg, 2011). A pyroxenite residue has been proposed for HMA lavas from the central Mexican Volcanic Belt (MVB), based on the anomalously high Ni contents of their olivine phenocrysts (Straub *et al.*, 2008, 2011). Comparison of olivine from pyroxenite-derived HMA (e.g. the central MVB HMA) and those from peridotite-derived basalts shows that the former not only have high Ni concentrations but also follow steeper trends in a plot of Ni versus Fo (Straub *et al.*, 2008).

Although olivine phenocrysts from the Guiyunhua Ol-HMA have unusually high Ni contents compared with olivine crystallized from partial melts of a normal lherzolite source, they follow a shallower trend than those from pyroxenite-derived HMA in the central MVB in a Ni vs Fo plot (Fig. 5c). However, their compositions and Ni vs Fo trend are very similar to those of HMAs in the Setouchi volcanic belt, Japan (Tatsumi *et al.*, 2003), which have been interpreted to have equilibrated with mantle peridotite (Tatsumi, 1982, 2006). Consequently, the high-Ni olivines in the Guiyunhua HMA are considered to reflect melts that last equilibrated with a harzburgitic residue (Tatsumi *et al.*, 2006) or were generated from a peridotite source that experienced metasomatism by sulfur-bearing silicic melts before the melting event (Ishimaru & Arai, 2008), rather than melts derived from an olivine-free source.

A peridotitic, rather than a pyroxenitic, source for the Guiyunhua HMA is also supported by their chemical and isotopic compositions. The volcanic rocks have Sr–Nd isotope compositions not only distinct from those of pyroxenite xenoliths exhumed by contemporary basalts in the NCC (Fangcheng pyroxenites; Zhang *et al.*, 2008) but also those of early Cretaceous lavas in the Liaodong Peninsula, which have been interpreted to be derived from a pyroxenitic source (Pang *et al.*, 2015) (Fig. 10a); this suggests that their source probably was not a mantle pyroxenite. As shown in Fig. 11, comparison of the Guiyunhua Ol-HMA with high-pressure experimental melts of pyroxenite and hydrous peridotite further suggests that these HMAs cannot be derived from partial melting of either silica-deficient (SD) or silica-excess (SE) pyroxenite. For example, partial melting of SE pyroxenite can produce andesitic melts but with MgO lower than 8 wt % (Fig. 11a). To generate a high-MgO magma, an SD pyroxenitic source is required, but melts derived from such sources have lower silica (Fig. 11a) and higher FeO (Fig. 11b) than those of the Guiyunhua HMAs. Moreover, the Guiyunhua HMAs are more deficient in TiO_2 than melts of pyroxenite (either SD or SE types) (Fig. 11d), even though rutile was present as a

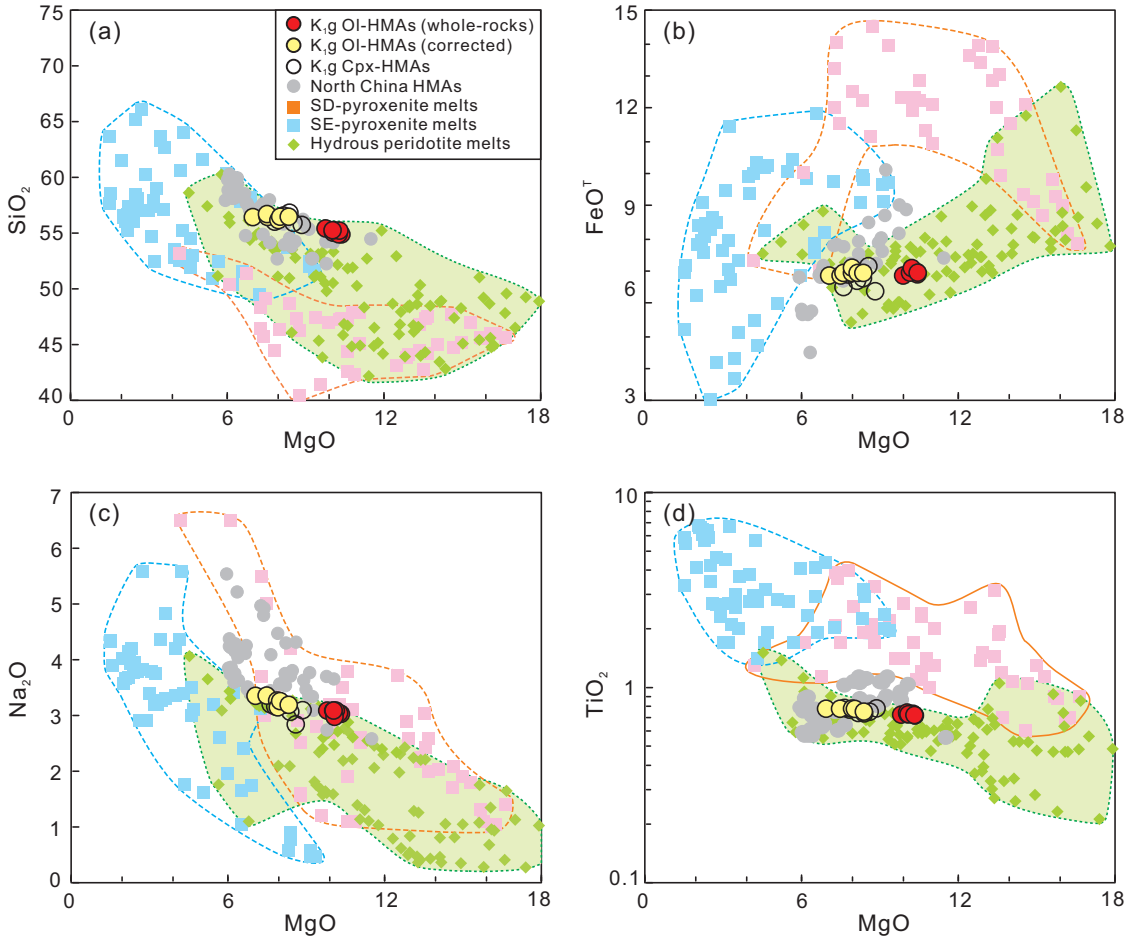

Fig. 11. Comparison of early Cretaceous Guiyunhua HMAs with high-pressure experimental melts of silica-excess (SE) pyroxenites, silica-deficient (SD) pyroxenites and hydrous peridotites (references to data source in Supplementary Data Electronic Appendix 2). Red- and yellow- filled circles are Ol-HMA whole-rock compositions and with a correction for phenocryst content, respectively. K_1g represents Early Cretaceous Guiyunhua volcanic rocks (LBGMR, 1989).

residual phase in some experiments. Such low TiO_2 concentrations in andesitic primary liquids can be ascribed to equilibration with a harzburgitic residue (refractory source or high-degree melting; Weaver *et al.*, 2011). The comparisons also suggest that the most plausible source is peridotite, because the Guiyunhua HMAs plot within the range defined by melts from hydrous melting of peridotite.

Melting conditions (P–T–X_{H2O})

The compositions of mafic magmas reflect the melting temperature and pressure of the magma source rock (Putirka *et al.*, 2007; Lee *et al.*, 2009), providing windows into the thermal state of the deep mantle. Accepting that peridotite is the likely source lithology of the Guiyunhua HMA, we have calculated the temperature and pressure of magma generation using the thermobarometers developed by Lee *et al.* (2009), which are applicable to melts in equilibrium with a residue containing both olivine and orthopyroxene. Our calculation of *P–T* conditions used the whole-rock compositions of the Ol-HMA and assumed that the residuum is lherzolite ($Fe^{3+}/Fe^{T}=0{\cdot}1$ and final olivine with Mg#$=90$) or harzburgite ($Fe^{3+}/Fe^{T}=0{\cdot}1$ and final olivine with Mg#$=92$). The results are presented in Fig. 12a and the effects of water (0, 3, 5 and 7 wt % H_2O) on *P* and *T* are also shown. Regardless of the choice of water content and residue, the calculated pressures are mostly less than 1·2 GPa, indicating melting of shallow (<40 km) mantle. All the pressures calculated assuming a lherzolitic residue are so low (<1 GPa; 0·67–0·92 GPa) that melting would appear to occur in the crust. This is clearly unreasonable and suggests that the Ol-HMA cannot be generated by anhydrous or hydrous (unless with $H_2O \geq 9\%$) melting of peridotite with a lherzolitic residue. However, calculations leaving a harzburgitic residue yield deeper and more reasonable melting depths (1·03–1·06 GPa and 1·07–1·20 GPa for anhydrous and hydrous mantle, respectively). Considering that the Guiyunhua HMAs are H_2O-rich magmas, and that the melting products of peridotite under anhydrous conditions are basalts

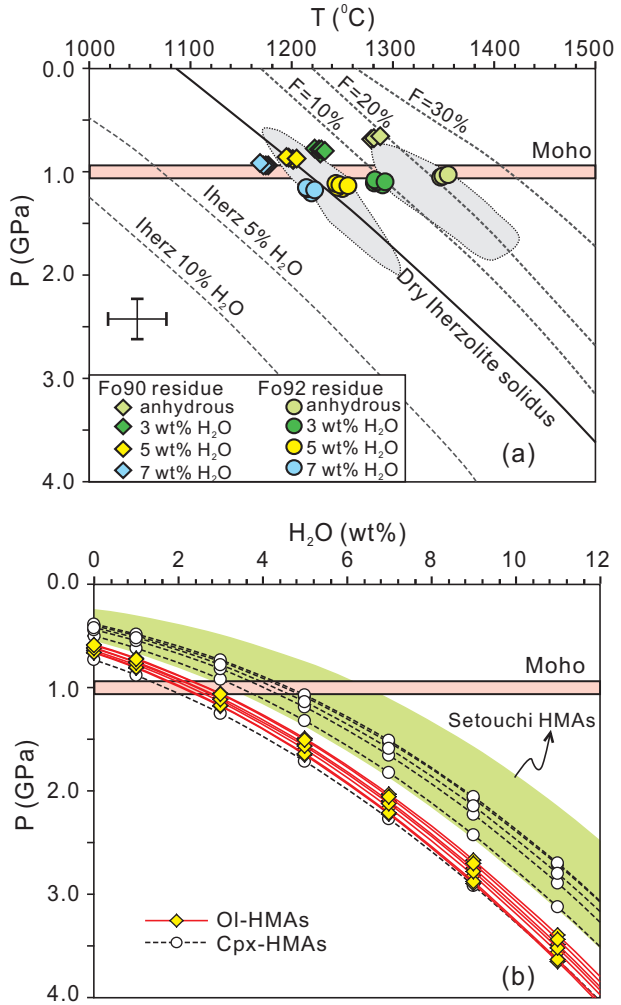

Fig. 12. Pressure, temperature and H_2O content (*P–T*–wt % H_2O X_{H2O}; Lee *et al.*, 2009; Wood & Turner, 2009) calculated for early Cretaceous Guiyunhua HMAs from the Liaodong Peninsula. Lherzolite solidi for varying water contents in (a) are taken from Katz *et al.* (2003). The grey fields in (a) are MORBs (right) and Izu-Bonin boninites (left) (Lee *et al.*, 2009). *P–*X_{H2O} calculation in (b) assumes: (1) melts could coexist with a harzburgitic residue; (2) adding 1 wt % H_2O into the system would decrease SiO_2 by 0·6 wt % and increase MgO by 1·0 wt %; (3) Cpx-undersaturation (harzburgitic residue) would decrease SiO_2 and MgO in the ratio 1:2. Detailed calculation procedures have been described by Wood & Turner (2009). The field of HMAs in the Setouchi volcanic belt, Japan, in (b) is calculated for TG1 and SD261 (Tatsumi, 1982).

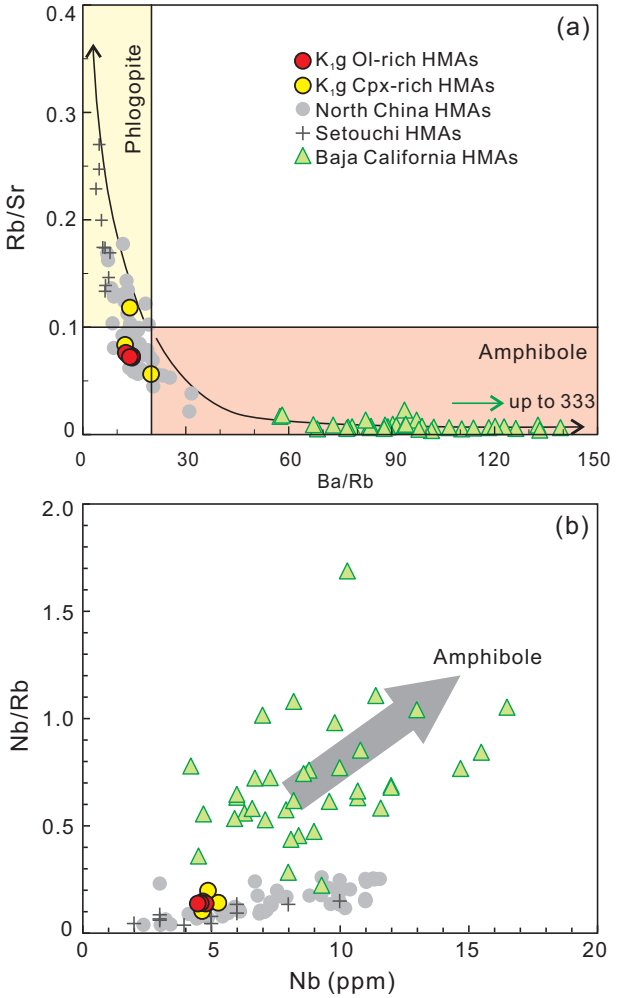

Fig. 13. Variation of Rb/Sr vs Ba/Rb (a) and Nb/Rb vs Nb (b) for early Cretaceous Guiyunhua volcanic rocks from the Liaodong Peninsula, North China. The trends labeled 'amphibole' and 'phlogopite' in (a) indicate that these two hydrous phases may be present in the mantle source of the magmas, respectively. Neogene HMAs in northern Baja California, which have been interpreted as melts of pargasite (amphibole)-rich lithospheric mantle, are from Pallares *et al.* (2008). K_1g represents Early Cretaceous Guiyunhua volcanic rocks (LBGMR, 1989).

rather than high-Mg andesites, we propose that the primary HMAs in the Liaodong Peninsula were derived from a hydrous peridotite at 1210–1290°C and 1·1–1·2 GPa, leaving behind a harzburgitic residue.

To constrain the water content in the Guiyunhua HMAs, we calculated the range of pressures and H_2O contents under which HMA melts would be in equilibrium with a harzburgitic residue, following the procedure developed by Wood & Turner (2009). Assuming melting pressures of 1·03–1·20 GPa based on *P–T* estimations, application of the thermobarometers of Lee *et al.* (2009) suggest that the Ol-HMAs were derived from a mantle peridotite with more than 3 wt % H_2O in the system (Fig. 12b). In summary, primitive HMA magmas in the Liaodong Peninsula were formed by hydrous ($H_2O > 3$ wt %) melting of a peridotitic mantle and last equilibrated with a harzburgitic residue at ~1250°C and ~1·1–1·2 GPa.

Crustal component in the Guiyunhua HMAs

The early Cretaceous Guiyunhua HMAs are enriched in LREE, LILE and Pb, with negative anomalies in HFSE relative to the primitive mantle (Fig. 8). It is generally accepted that most of the LREE, LILE and H_2O of HMA in subduction zones are contributed from subducted sediments and other crustal rocks (Shimoda *et al.*, 1998; Tatsumi, 2001; Grove *et al.*, 2002; Yogodzinski *et al.*,

2015). Alternatively, these components can be attributed to dehydration melting of pargasite-rich lithospheric mantle (Pallares *et al.*, 2008). However, the Guiyunhua HMAs in the Liaodong Peninsula, as well as contemporary HMAs and diorites from the NCC, have low Ba/Rb and Nb/Rb and low Nb contents (Fig. 13), which are inconsistent with melting of an amphibole-rich mantle source (Furman & Graham, 1999; Pallares *et al.*, 2008). Thus, the addition of crust-derived components probably induced hydrous melting and selective enrichment of incompatible elements in the source of the Guiyunhua HMAs. In the following discussion we address the possible nature of the crustal components involved in the genesis of the high-Mg magmas using isotopic and trace element modeling.

Traditionally, the depleted mantle is taken as the mantle end-member in mass-balance modeling of HMAs in a subduction zone (e.g. Grove *et al.*, 2002; Yogodzinski *et al.*, 2015). However, this practice may not be appropriate because the Guiyunhua HMAs may be melts of enriched SCLM beneath the NCC (Fig, 10). Detailed geochemical and isotopic studies show that 130–110 Ma mafic igneous rocks in the eastern NCC were overwhelmingly derived from ancient and enriched lithospheric mantle (Xu, 2001; Xu *et al.*, 2009). Asthenosphere-derived mafic magmas occur only locally, such as the lamprophyre dikes in Shandong Province (Ma *et al.*, 2014). However, these lamprophyres have high TiO_2 (>2 wt %), in contrast to the low TiO_2 (<0·8 wt %) of the Guiyunhua HMAs, reflecting their different mantle sources.

The Guiyunhua lavas have enriched Sr–Nd isotope compositions, comparable with those of peridotite xenoliths and perovskite from the Paleozoic Fuxian and Mengyin (~465 Ma; Zhang & Yang, 2007) kimberlites (SCLM in Fig. 10a), consistent with derivation from the ancient SCLM beneath the NCC. The application of the thermobarometers also indicates that the Guiyunhua HMAs could have been in equilibrium with mantle peridotite at 1·1–1·2 GPa, corresponding to a lithospheric mantle depth. Accordingly, we used the Sr–Nd isotopic composition of perovskite in the Ordovician kimberlites (recalculated to 122 Ma) as representative of the SCLM beneath the NCC. The trace element composition of the SCLM prior to Phanerozoic modification is based on the compositions of peridotite xenoliths in Paleozoic Fuxian kimberlites in the Liaodong Peninsula (Lu & Zheng, 1996; Zhang *et al.*, 2008; Fig. 1b). A mantle end-member with the trace element composition of depleted MORB mantle was also considered for the purpose of comparison.

The Guiyunhua HMAs do not have trace element compositions consistent with derivation from SCLM represented by the peridotite xenoliths in kimberlites (Fig. 14), and thus additional metasomatic or crustal components are required. The NCC experienced multiple oceanic and continental subduction episodes during Phanerozoic time (Windley *et al.*, 2010). Hence, the crustal component(s) in the Guiyunhua HMA magmas were probably introduced from subducted oceanic crust, marine sediments, continental sediments and Yangtze continental crust. Foundered eclogitic lower continental crust of the NCC also needs to be considered, as lithospheric delamination is thought to be responsible for Mesozoic magmatism in the NCC (Gao *et al.*, 2004, 2008; Wu *et al.*, 2005*a*; Xu *et al.*, 2008). We assume that crustal materials are not transferred 'in bulk' to the lithospheric mantle, but selectively via infiltration of partial melts, fluids or supercritical liquids into the mantle (Kessel *et al.*, 2005; Skora & Blundy, 2010; Straub *et al.*, 2015) creating a hybrid source for the HMA magmas. We consider for simplicity the case in which the crustal component involved in generation of the Guiyunhua HMA is in the form of a partial melt. Details of the parameters used in the modeling, including the compositions of end-members, enrichment factors of sediment melt, mobility of slab melt and melts of recycled lower continental crust, are listed in Supplementary Data Electronic Appendix 3. The modeling results are shown in Fig. 14. It is worth noting that our modeling does not consider contributions from crustal aqueous fluids and that the hypothetical trace element compositions of the mantle end-members are poorly constrained. As a result, the modeling may capture only the first-order behavior of interaction between crustal components and mantle peridotite; the proportion of each crustal component in the models may represent only maximum estimates.

The Guiyunhua volcanic rocks plot far away from the mixing curves between oceanic slab melts and any mantle end-member, suggesting that subducted oceanic crust played an insignificant role in their generation. This argument is further supported by the low Sr/Y (<32; Fig. 9a) and La/Yb (<13; Fig. 8a) of the rocks. Although recycled lower continental crust (both from foundered lower crust of the NCC and deeply subducted Yangtze lower crust) can explain the radiogenic Sr isotope compositions (Fig. 14a and d), low Ta/Th (Fig. 14 and e) and high Ba/Nb ratios (Fig. 14c and f), this component would have low $\varepsilon_{Nd}(t)$ and Th/La, which is inconsistent with those of the Guiyunhua HMAs. Furthermore, lower continental crust beneath eastern China is refractory and nearly anhydrous (Liu *et al.*, 2001; Zhai *et al.*, 2001; Zheng *et al.*, 2004; Jiang *et al.*, 2013), and therefore, if recycled, this lower crust could not supply enough water to induce hydrous melting of the lithospheric mantle. The involvement of subducted sediments can reasonably explain the isotopic and incompatible trace element characteristics of the high-Mg lavas. As shown in Fig. 14, all the mixing curves between mantle end-members and melts of global subducted sediment (GLOSS) pass though the Guiyunhua HMA data. Another candidate for the recycled sediment component may be subducted continental sediment from the Yangtze block. There is a time span of ~100 Myr between collision between the NCC and the Yangtze block (Li *et al.*, 1993) and the Early Cretaceous magmatism. One plausible scenario is that the enriched

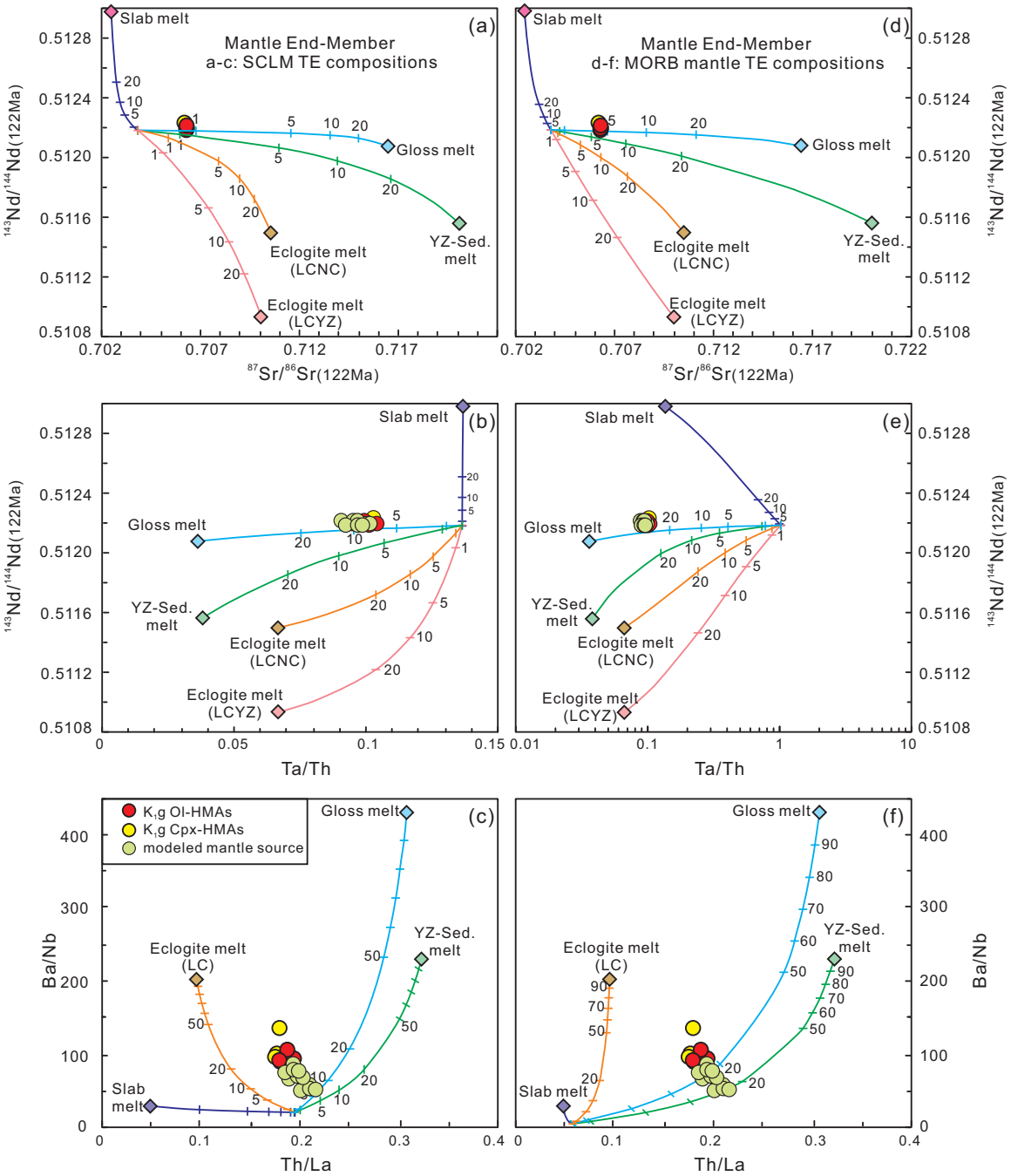

Fig. 14. Variation of $^{143}Nd/^{144}Nd$ vs $^{87}Sr/^{86}Sr$ (a, d) $^{143}Nd/^{144}Nd$ vs Ta/Th (b, e) and Ba/Nb vs Th/La (c, f) for early Cretaceous Guiyunhua volcanic rocks from the Liaodong Peninsula, compared with mixing trends between mantle peridotite and crust-derived melts. The mantle source of HMAs is modeled at 10%, 20% and 30% batch melting of peridotite with a harzburgitic residue (Supplementary Data Electronic Appendix 3). The Sr–Nd isotope composition of the SCLM mantle end-members is based on perovskite in Paleozoic kimberlites in the NCC. The trace-element compositions of the mantle end-member (SCLM) used in (a–c) and MORB mantle (d–f) are based on those of peridotite xenoliths in Paleozoic Fuxian kimberlites from the Liaodong Peninsula and those of the depleted mantle, respectively. Detailed parameters used in the modeling are listed in Supplementary Data Electronic Appendix 3. It should be noted that the geochemical modeling presented here does not consider the contributions from crustal (slab and sediment) fluids, so the proportions of the crustal components in the modeling may represent maximum estimates.

mantle was produced by interaction between sediment-derived melts and peridotite during the Triassic or by late Archean–Palaeoproterozoic metasomatic events (Pang *et al.*, 2015), and was subsequently melted in the Cretaceous, triggered by rollback of the subducting paleo-Pacific slab (Zhao *et al.*, 2013). Consequently, we propose that the crustal component involved in the generation of the Guiyunhua HMAs was derived from either

more recently subducted sediments (i.e. during paleo-Pacific subduction) or ancient subducted materials (e.g. Yangtze sediments).

Genesis of the Cpx-HMAs

The Guiyunhua HMAs are subdivided into Ol-HMA and Cpx-HMA according to their petrography and geochemistry. As mentioned above, the former can be taken as primary or near-primary magmas that last equilibrated with mantle peridotite. The latter are interpreted as having differentiated from the Ol-HMA by olivine-dominated fractionation in association with minor assimilation of lower crustal materials. The main evidence includes the following.

1. The Cpx-HMAs have lower MgO, FeO^T and Ni than the Ol-HMAs (Figs 6 and 7), indicating that olivine was a dominant fractionating phase.
2. Olivine phenocrysts in the Cpx-HMAs have lower Fo and Ni contents, but higher CaO than those in the Ol-HMAs (Figs 4 and 5), suggesting that they are late-crystallizing phases.
3. Clinopyroxene fractionation seems to be insignificant, judging from invariant CaO (Fig. 6b) and Cr (Fig. 6h) with decreasing MgO. The compositional difference between the Cpx phenocrysts from the two types of HMA is attributed to different equilibrium melts; more differentiated magmas would have lower Mg# and higher water contents.
4. Fe–Ti oxide fractionation may have occurred, as reflected in the presence of magnetite as phenocrysts and a groundmass mineral in the Cpx-HMAs (Supplementary Data Fig. S3 in Electronic Appendix 4). However, fractionation of Fe–Ti oxides was not appreciable, considering the similar TiO_2 concentrations of the two types of HMA. In addition, most of the magnetite observed in the Cpx-HMAs is a product of reaction between xenocrystic Cpx and the surrounding melt.
5. The occurrence and compositions of green-cored clinopyroxene phenocrysts (Fig. 2d; Supplementary Data Fig. S4 in Electronic Appendix 4) suggest that contamination by lower crustal rocks was involved in the genesis of the Cpx-HMA lavas. However, the homogeneous trace element (Fig. 8) and Sr–Nd isotope compositions (Fig. 10a) of the Guiyunhua high-Mg volcanic rocks indicate that lower-crustal contamination or assimilation could have played only a limited role, at least in terms of trace element and isotopic compositions, during evolution of the magmas.

Petrogenesis of the Guiyunhua adakitic rocks

Origin of the adakitic geochemical signature

As discussed above, the trace element characteristics of the Guiyunhua dacites are broadly similar to those of adakites in modern subduction zones (Defant & Drummond, 1990). These lavas have high SiO_2 ($\geq$63 wt %) and K_2O (>1·3 wt %), low Rb/Ba ($\leq$0·1), Nb/U (<12) and Ce/Pb (<7), and unradiogenic whole-rock Nd isotope [$\varepsilon_{Nd}(t) = -19$ to -9; Fig. 10a] and zircon Hf isotope [$\varepsilon_{Hf}(t) = -22{\cdot}8$ to $-21{\cdot}1$; Fig. 10b] compositions that are consistent with their derivation from ancient mafic lower crust. Such adakitic rocks in continental settings are commonly regarded as the products of melting of thickened or foundered mafic lower continental crust (LCC) at depths greater than 50 km (Xu *et al.*, 2002; Chung *et al.*, 2003; Gao *et al.*, 2004). These premises are built on experiments and modeling using a MORB-like source (Xiong *et al.*, 2005; Nair & Chacko, 2008), which is obviously not the case for such continental adakitic rocks (Ma *et al.*, 2012, 2015). Recent experiments (Qian & Hermann, 2013) and trace element modeling (Ma *et al.*, 2015) have shown that adakitic melts can be produced by lower-pressure (10–12·5 kbar) melting of mafic lower crust, without leaving eclogitic residues. Ma *et al.* (2015) highlighted that the adakitic geochemical signatures of igneous rocks from cratonic areas and collisional orogens are mainly controlled by inheritance from the geochemical signatures of their source and high-pressure melting, respectively. A $(Sm/Yb)_{SN}$ vs Yb_{SN} diagram (where the subscript SN denotes source-normalized) can be used to evaluate the relative contributions of source inheritance versus high-*P* melting in their generation. The Guiyunhua adakitic dacites have low $(Sm/Yb)_{SN}$ and high Yb_{SN}, similar to intraplate adakitic rocks that were generated at depths less than 40 km (Fig. 9b). Therefore, we propose that the main compositional characteristics of the Guiyunhua adakitic lavas (e.g. high Sr/Y, Nb–Ta depletion, lack of Eu anomaly and low HREE contents) are inherited from their source rocks (i.e. mafic lower continental crust of the NCC), rather than reflecting melting at high pressure ($\geq$1·5 GPa).

Other independent evidence for lower crustal melting at depths less than 40 km comes from the pressure estimation for the coeval HMAs (Fig. 12). As discussed above, the Guiyunhua HMAs were derived from a wet peridotite mantle at 1·1–1·2 GPa, indicating that the maximum thickness of crust beneath the Liaodong Peninsula would not have exceeded 40 km at the time of magma generation. Most of the Guiyunhua dacites are low-Mg adakitic dacites with low MgO (<1·2 wt %), Mg# (<41), Ni (<7 ppm) and Cr (<20 ppm), which indicate that they were directly derived from lower-crustal rocks rather than being melts of foundering eclogites at mantle depths. Moreover, these adakitic lavas were developed in association with late Mesozoic metamorphic core complexes and erupted in fault-bounded extensional basins (Fig. 1b; Liu *et al.*, 2013). Detailed studies on the coexistence of Cretaceous volcanic–sedimentary basins, low-angle normal faults, exhumed high-grade metamorphic rocks with early Cretaceous cooling ages, and widespread A-type granitoids in the lower plate of the MCC demonstrate that the crust of the Liaodong Peninsula was relatively thin and experienced exceptionally intense extension during early Cretaceous times (Liu *et al.*, 2005, 2011, 2013). Therefore, no

thickened lower crust is likely to have been present in the study area at that time; correspondingly, the melting of lower continental crust probably occurred at depths <40 km.

Generation of high-Mg adakitic dacites by magma mixing

The Guiyunhua high-Mg adakitic dacites (SHY14 and SHY15) have higher Mg# (>51), Ni (~53 ppm) and Cr (~112 ppm) than the low-Mg adakitic dacites and experimental melts equilibrated with basaltic rocks at 1–4 GPa (Rapp *et al.*, 1999; Qian & Hermann, 2013). Three scenarios have been proposed to account for the high-Mg signature of Mesozoic adakitic rocks in the NCC: (1) interaction of melts derived from foundered lower crust with mantle peridotite as they ascended (Gao *et al.*, 2004); (2) underplated mafic melts incorporated into adakitic magmas in deep crustal hot zones (Ma *et al.*, 2012); (3) mixing of basaltic and felsic magmas in a magma chamber (Chen *et al.*, 2013). The first hypothesis can be ruled out as we have demonstrated that there was no thickened or foundered lower crust beneath the Liaodong Peninsula when the Guiyunhua lavas were erupted. Although it is difficult to distinguish between the other two processes using available geochemical data, we favor the possibility of magma mixing in a magma chamber on the basis of the estimated crystallization depth. The amphibole phenocrysts record low crystallization temperatures (836–895°C) and shallow crystallization depth (1·4–5·0 kbar) (Table 5). In contrast, clinopyroxene phenocrysts that are rimmed by amphibole record a higher crystallization temperature (1089–1110°C) and deeper crystallization depths (4·5–6·9 kbar) according to the clinopyroxene–liquid thermobarometer for hydrous systems (Putirka *et al.*, 2003); these conditions are similar to the crystallization *P–T* of the Cpx-HMAs. Thus, the mafic and felsic magmas would have mixed at mid- to upper-crustal levels rather than in a hot zone near the crust–mantle boundary. Most plausibly, the mixing components would be the low-Mg adakitic dacitic magmas and the differentiated Cpx-HMAs. This argument is supported by the fact that the high-Mg dacites plot between the HMAs and the low-Mg adakitic dacites in Harker diagrams (Fig. 7), chondrite-normalized REE diagrams (Fig. 8a) and primitive mantle-normalized trace element diagrams (Fig. 8b) and in terms of initial Sr–Nd isotope composition (Fig. 10a).

Probable heat sources: underplated mafic magma

The source of heat for melting the lower crust beneath the NCC in late Mesozoic time is an important, but open, question. Because ancient lower continental crust (LCC) is composed of granulite-facies rocks that are depleted in heat-producing elements (Rudnick & Gao, 2003), heat accumulating from the radioactive decay of such elements cannot account for melting of the lower crust beneath the NCC. Thus, the heat should be exotic, either from upwelling asthenospheric mantle (Wu *et al.*, 2005*a*), or from underplating basaltic magmas (Ma *et al.*, 2012, 2015), or both (Wu *et al.*, 2005*b*). Upwelling of asthenospheric mantle would not only heat the overlying lithosphere, but also result in large-scale basaltic magmatism by decompression melting. Nevertheless, early Cretaceous mafic igneous rocks in the eastern NCC appear to be overwhelmingly derived from enriched lithospheric mantle (Xu, 2001; Xu *et al.*, 2009). Mafic magmas derived from the asthenosphere occur only locally as lamprophyre dikes in Shandong Province (Ma *et al.*, 2014). Accordingly, partial melting of the lower crust beneath the NCC probably was not due to direct heating by upwelling of asthenospheric mantle. Episodic underplating of magma at the base of the lower crust during late Mesozoic times (160–66 Ma with a peak at ~120 Ma) has been recognized by studies of contemporary igneous rocks (Yang *et al.*, 2006; Yang & Li, 2008) and xenoliths in Cenozoic basalts (Liu *et al.*, 2004; Zheng *et al.*, 2012; Zhang *et al.*, 2013). Hf isotope compositions of magmatic zircons from late Mesozoic lower crust-derived granitoids indicate significant addition of juvenile crust by underplating of magmas beneath the Liaodong Peninsula (Yang *et al.*, 2008). Therefore, underplating of basaltic and/or HMA magmas represents the most plausible heat source for melting of the lower crust beneath the NCC.

The rarity of hydrous phases in lower crustal rocks from the NCC suggests that the lower crust is essentially refractory and anhydrous (Liu *et al.*, 2001; Zhai *et al.*, 2001; Zheng *et al.*, 2004; Jiang *et al.*, 2013). Furthermore, zircon-saturation temperatures suggest that the initial magma temperatures of late Mesozoic I-type granitoids in the Liaodong Peninsula were 750–800°C (Wu *et al.*, 2007), which is much lower than that of amphibole-dehydration melting reactions (Weinberg & Hasalová, 2015). As a result, melting of anhydrous lower crust by heating alone cannot produce the widespread late Mesozoic felsic igneous rocks in the eastern part of the NCC. Rather, these crustal magmas could have been formed by water-fluxed melting of the lower crust. We therefore speculate that the underplated magmas provided not only heat but also (and perhaps more importantly) additional water.

The candidate for the underplated magma beneath the Liaodong Peninsula is the HMA melts that were derived from the upper lithospheric mantle (Fig. 12) and were emplaced into the base of the crust (Table 5). As discussed above, the primary Guiyunhua Ol-HMAs are hydrous magmas that once equilibrated with the upper mantle in the presence of more than 3% water. However, their differentiation products (Cpx-HMAs) are phenocryst-poor, corresponding to relatively dry magmas. In this respect, the Guiyunhua HMAs are very similar to the sanukitoids from the Setouchi volcanic belt, southwestern Japan. Tatsumi *et al.* (2006) proposed that liberation of H_2O from hydrous HMA magmas in association with pluton solidification could explain this apparent paradox. If a similar scenario

applies to the Guiyunhua case, then the extracted water could have been added to the overlying lower crust, triggering water-fluxed melting of this previously anhydrous lower crust.

Summary of petrogenesis of the Guiyunhua HMAs and adakitic dacites

To summarize the above discussion, we consider the petrogenesis of the Guiyunhua HMAs and adakitic dacites in the Liaodong Peninsula in the following stages.

1. Generation of primary high-Mg andesites (Ol-HMAs) by hydrous ($H_2O > 3$ wt %) melting of lithospheric mantle, leaving a harzburgitic residue at ~1250°C and ~1·1–1·2 GPa.
2. Emplacement of the HMA magmas into the lower crust as a succession of sill-like bodies leading to the generation of a deep-crustal hot zone. Solidification of HMA plutons was accompanied by olivine-dominated fractionation, minor lower crustal assimilation and extraction of H_2O at 0·7–1·1 GPa, which led to the formation of differentiated HMAs (Cpx-HMAs).
3. Release of heat and H_2O from hydrous HMA magmas promoted partial melting of ancient lower crust, and generation of low-Mg adakitic magmas.
4. Mixing between differentiated Cpx-HMA and low-Mg adakitic magmas in magma chambers resulted in high-Mg adakitic dacites.

This petrogenetic model explains the Mesozoic HMA and adakitic magmas in the NCC and elsewhere. Because ascent of water-rich magmas would be inhibited by decompression crystallization accompanying the loss of volatiles, most of the HMAs and adakitic rocks in the NCC would solidify within the crust. This expectation is consistent with the observation that widespread Mesozoic adakitic and HMA igneous rocks in the NCC occur as plutonic intrusions (i.e. adakitic granitoids and high-Mg diorites) rather than as their volcanic equivalents (i.e. adakitic and HMA lavas).

Geodynamic implications

Destruction of the North China Craton

Ancient cratons, the most stable parts of the continents, are underlain by thick thermal and mechanical boundary layers that have been largely isolated from the convective asthenospheric mantle over billion year timescales (Kelly *et al.*, 2003; Carlson *et al.*, 2005; Lee *et al.*, 2011). However, several lines of evidence suggest that the eastern part of the NCC has been destroyed since the Phanerozoic (Menzies *et al.*, 1993; Griffin *et al.*, 1998; Xu, 2001; Gao *et al.*, 2002; Wu *et al.*, 2003; Zheng *et al.*, 2007). Constraining the thermal regime of the lithosphere at different times (Menzies & Xu, 1998; Xu, 2001; Huang & Xu, 2010) is crucial to address the timing and mechanism of the destruction of this craton. The lithosphere of the NCC is characterized by a low geothermal gradient in the Paleozoic (~40 mW m^{-2}; Griffin *et al.*, 1998; Zheng *et al.*, 2006) and by a high geothermal gradient in the Cenozoic (~80 mW m^{-2}; Xu *et al.*, 1995; Menzies & Xu, 1998; Xu *et al.*, 1998; Xu, 2001; Zheng *et al.*, 2006) (Fig. 15). It is been suggested that the heat flow in the eastern NCC reached ~90 mW m^{-2} in the early Tertiary (Fig. 15; He, 2015) and peaked in the Mesozoic (>100 mW m^{-2}) (Menzies & Xu, 1998). However, there is no valid constraint on the thermal state of the SCLM beneath the NCC during the Mesozoic, mainly owing to the lack of garnet-bearing peridotite xenoliths in contemporary basalts. To address this issue, we compared the depth and temperature of mantle melting that generated the early Cretaceous Guiyunhua HMAs with the Paleozoic, early Tertiary and present-day thermal regime of the NCC. As shown in Fig. 15, the lithospheric mantle beneath the NCC is hottest in early Cretaceous time, corresponding to the peak of lithospheric thinning and cratonic destruction (Xu *et al.*, 2009). The early Cretaceous thermal anomaly is consistent with intensive magmatism, extensional deformation and associated gold mineralization (Wu *et al.*, 2005*a*; Zhu *et al.*, 2012*b*, 2015).

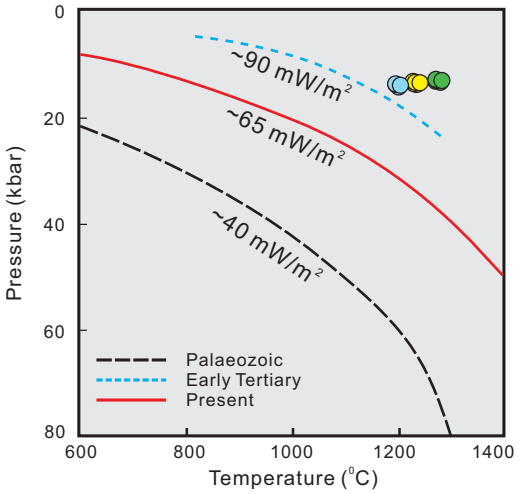

Fig. 15. Comparison of the depths and temperatures of generation of the early Cretaceous Guiyunhua HMAs (dots) with Palaeozoic, early Tertiary and present-day geotherms of the NCC (Griffin *et al.*, 1998; Xu, 2001). The blue, yellow and green dots are calculated based on 7 wt %, 5 wt % and 3 wt % H_2O in the system, respectively (see Fig. 12 and main text).

The mechanisms of destruction of the lithospheric mantle beneath the NCC have been long debated (Zheng, 1999; Xu, 2001, 2007; Gao *et al.*, 2004; Wu *et al.*, 2005*a*; Zheng *et al.*, 2007, 2015; Zhang *et al.*, 2008; Zhang, 2009; Tang *et al.*, 2013). As discussed above, the early Cretaceous HMAs and felsic adakitic rocks in the NCC appear to be produced by hydrous melting of shallow, hot and refractory peridotitic mantle and by water-fluxed melting of ancient lower crust, respectively. Specifically, the generation of the Guiyunhua HMAs involved more than 3 wt % H_2O in the system (Fig. 12), suggesting high water contents in the early Cretaceous lithospheric mantle beneath the NCC. Such high water contents in the SCLM are also evidenced from

contemporary basalts in Shandong Province (>1000 ppm; Xia *et al.*, 2013). Hydration of the lithosphere may not only significantly reduce the viscosity contrast between the lithospheric mantle and the underlying asthenosphere (Niu, 2005; Lee *et al.*, 2011; Xia *et al.*, 2013), but also promote refertilization-driven destabilization of the craton (Kusky *et al.*, 2014; Zheng *et al.*, 2015; Xiong *et al.*, 2015). Therefore, we propose that destruction of the NCC was caused by erosion, replacement, modification or partial melting associated with the hydration of the lithosphere. A large amount of water was probably added to the lithospheric mantle during the multiple episodes of subduction that occurred around the eastern NCC since the early Paleozoic (Windley *et al.*, 2010; Xia *et al.*, 2013; Kusky *et al.*, 2014), and especially the rapid, deep subduction of the paleo-Pacific (Izanaghi) plate underneath East Asia (Niu, 2005; Zhao *et al.*, 2007; Xu *et al.*, 2012; Zhu *et al.*, 2012*c*; He, 2014; Xu, 2014). Rollback of the subducted paleo-Pacific slab during the early Cretaceous (Zhu *et al.*, 2012*a*; Kusky *et al.*, 2014) induced upwelling of the asthenosphere and vigorous convection, which could erode already refertilized lithospheric mantle within the mantle wedge (He, 2014), in association with widespread magmatism (e.g. Wu *et al.*, 2005*a*, and this study) and crustal extension (e.g. Liu *et al.*, 2013). As a result, destruction of the cratonic root probably attained its climax at that time.

Formation of Archean continental crust

The Archean continental crust is largely made up of granitoid gneisses, dominantly TTG series (Jahn *et al.*, 1981; Moyen & Martin, 2012) with subordinate Archaean sanukitoids (Shirey & Hanson, 1984; Martin *et al.*, 2005) and minor biotite and two-mica granites (Laurent *et al.*, 2014). Considering the close geochemical similarities between the TTG suites and modern adakites, and between Archaean sanukitoids and modern HMAs, Archean granitoids are widely used as a geodynamic indicator of the onset of 'modern-style' plate tectonics (Martin, 1999; Martin *et al.*, 2005; Laurent *et al.*, 2014). This hypothesis is mostly based on the observation that HMAs and adakitic lavas exclusively occur in hot subduction zones in the modern Earth (Defant & Drummond, 1990; Yogodzinski *et al.*, 1995; Grove *et al.*, 2002; Tatsumi, 2006), where a high-temperature regime leads to slab melting and transport of significant quantities of water into the mantle wedge. In this study we have shown that the early Cretaceous HMAs and adakitic rocks from the NCC formed in an intraplate extensional environment accompanied by the development of MCCs, low-angle normal faults and fault-bounded extensional basins (Liu *et al.*, 2013; Ji *et al.*, 2015). Archean TTGs and sanukitoids are actually rather ambiguous as a subduction marker (Moyen, 2011), as they can be produced in tectonic environments unrelated to plate boundaries, such as the progressive maturation of an oceanic plateau above a long-lived mantle plume (e.g. Smithies, 2000; Bédard, 2006; Willbold *et al.*, 2009; Reimink *et al.*, 2014) and in post-orogenic or anorogenic settings (e.g. Lobach-Zhuchenko *et al.*, 2008; Heilimo *et al.*, 2010). Therefore, caution is needed in using the occurrence of ancient HMA and adakitic magmas as an indicator of subduction processes.

CONCLUSIONS

1. Coeval HMAs and adakitic dacites in a continental setting are identified in the Liaodong Peninsula from the North China Craton. The early Cretaceous HMAs were derived from partial melting of shallow (1·1–1·2 GPa), hot (~1250°C) and wet (H_2O > 3 wt %) lithospheric mantle, leaving a harzburgitic residue. The associated adakitic rocks were formed by water-fluxed melting of ancient lower crust at depths of less than 40 km, induced by heating and H_2O addition from underplated hydrous mafic magmas (e.g. HMAs).
2. Early Cretaceous HMAs of the Liaodong Peninsula indicate high temperatures and high water contents in the SCLM beneath the craton at that time. Hydration of the lithosphere may be an important process or even a prerequisite for the destruction of a craton.
3. The generation of HMAs and adakitic magmas in an intraplate extensional environment indicates the need for caution in taking the occurrence of magmas with similar compositions as an indicator of ancient subduction processes.

SUPPLEMENTARY DATA

Supplementary data for this paper are available at *Journal of Petrology* online.

FUNDING

This work was supported by Strategic Priority Research Program (B) of Chinese Academy of Sciences (XDB18030604), National Natural Science Foundation of China (NSFC) grants (41502040, 41520104003, 41130315, 91014007 and 91214204) and National Key Research and Development Program of China (2016YFC0600103).

ACKNOWLEDGEMENTS

We thank Feng Guo, Shaokui Pan, Jiangtao Guo and Xianquan Ping for discussions and help in fieldwork. This paper benefited greatly from significant and constructive comments from Drs P. Castillo, T. Waight and an anonymous reviewer. This is contribution No. IS-2251 from GIG-CAS, 818 from the ARC Centre of Excellence for Core to Crust Fluid Systems, and 1083 from the GEMOC Key Centre.

REFERENCES

Amelin, Y. & Davis, W. J. (2005). Geochemical test for branching decay of ^{176}Lu. *Geochimica et Cosmochimica Acta* **69**, 465–473.

Anderson, J. L. & Smith, D. R. (1995). The effects of temperature and fO_2 on the Al-in-hornblende barometer. *American Mineralogist* **80**, 549–559.

Annen, C. & Sparks, R. S. J. (2002). Effects of repetitive emplacement of basaltic intrusions on thermal evolution and melt generation in the crust. *Earth and Planetary Science Letters* **203**, 937–955.

Annen, C., Blundy, J. D. & Sparks, R. S. J. (2006). The genesis of intermediate and silicic magmas in deep crustal hot zones. *Journal of Petrology* **47**, 505–539.

Bédard, J. H. (2006). A catalytic delamination-driven model for coupled genesis of Archaean crust and sub-continental lithospheric mantle. *Geochimica et Cosmochimica Acta* **70**, 1188–1214.

Blichert-Toft, J. & Albarède, F. (1997). The Lu–Hf isotope geochemistry of chondrites and the evolution of the mantle–crust system. *Earth and Planetary Science Letters* **148**, 243–258.

Carlson, R. W., Pearson, D. G. & James, D. E. (2005). Physical, chemical, and chronological characteristics of continental mantle. *Reviews of Geophysics* **43**, G1001.

Castillo, P. (2006). An overview of adakite petrogenesis. *Chinese Science Bulletin* **51**, 257–268.

Castillo, P. R. (2012). Adakite petrogenesis. *Lithos* **134–135**, 304–316.

Castillo, P. R., Janney, P. E. & Solidum, R. U. (1999). Petrology and geochemistry of Camiguin Island, southern Philippines: insights to the source of adakites and other lavas in a complex arc setting. *Contributions to Mineralogy and Petrology* **134**, 33–51.

Chen, B., Jahn, B. & Suzuki, K. (2013). Petrological and Nd–Sr–Os isotopic constraints on the origin of high-Mg adakitic rocks from the North China Craton: Tectonic implications. *Geology* **41**, 91–94.

Chiaradia, M. (2015). Crustal thickness control on Sr/Y signatures of recent arc magmas: an Earth scale perspective. *Scientific Reports* **5**, 8115.

Chung, S. L., Liu, D. Y., Ji, J. Q., Chu, M. F., Lee, H. Y., Wen, D. J., Lo, C. H., Lee, T. Y., Qian, Q. & Zhang, Q. (2003). Adakites from continental collision zones: Melting of thickened lower crust beneath southern Tibet. *Geology* **31**, 1021–1024.

Crawford, A. J., Falloon, T. J. & Green, D. H. (1989). Classification, petrogenesis and tectonic setting of boninites. In: Crawford, A. J. (ed.) *Boninites and Related Rocks*. Unwin Hyman, pp. 1–49.

Defant, M. J. & Drummond, M. S. (1990). Derivation of some modern arc magmas by melting of young subducted lithosphere. *Nature* **347**, 662–665.

Foley, S. F., Prelevic, D., Rehfeldt, T. & Jacob, D. E. (2013). Minor and trace elements in olivines as probes into early igneous and mantle melting processes. *Earth and Planetary Science Letters* **363**, 181–191.

Furman, T. & Graham, D. (1999). Erosion of lithospheric mantle beneath the East African Rift system: geochemical evidence from the Kivu volcanic province. *Lithos* **48**, 237–262.

Gaetani, G. A., Grove, T. L. & Bryan, W. B. (1993). The influence of water on the petrogenesis of subduction related igneous rocks. *Nature* **365**, 332–334.

Gao, S., Rudnick, R. L., Carlson, R. W., McDonough, W. F. & Liu, Y. S. (2002). Re–Os evidence for replacement of ancient mantle lithosphere beneath the North China craton. *Earth and Planetary Science Letters* **198**, 307–322.

Gao, S., Rudnick, R. L., Yuan, H. L., Liu, X. M., Liu, Y. S., Xu, W. L., Ling, W. L., Ayers, J., Wang, X. C. & Wang, Q. H. (2004). Recycling lower continental crust in the North China craton. *Nature* **432**, 892–897.

Gao, S., Rudnick, R. L., Xu, W. L., Yuan, H. L., Liu, Y. S., Walker, R. J., Puchtel, I. S., Liu, X. M., Huang, H., Wang, X. R. & Yang, J. (2008). Recycling deep cratonic lithosphere and generation of intraplate magmatism in the North China Craton. *Earth and Planetary Science Letters* **270**, 41–53.

Griffin, W. L., Zhang, A., O'Reilly, S. Y. & Ryan, C. G. (1998). Phanerozoic evolution of the lithosphere beneath the Sino-Korean craton. In: Flower, M. J., Chung, S. L., Lo, C. H. & Lee, T. Y. (eds) *Mantle Dynamics and Plate Interactions in East Asia. American Geophysical Union, Geodynamic Series* **27**, 107–126.

Griffin, W. L., Pearson, N. J., Belousova, E., Jackson, S. E., Van Achterbergh, E., O'Reilly, S. Y. & Shee, S. R. (2000). The Hf isotope composition of cratonic mantle: LAM-MC-ICPMS analysis of zircon megacrysts in kimberlites. *Geochimica et Cosmochimica Acta* **64**, 133–148.

Grove, T., Parman, S., Bowring, S., Price, R. & Baker, M. (2002). The role of an H_2O-rich fluid component in the generation of primitive basaltic andesites and andesites from the Mt. Shasta region, N California. *Contributions to Mineralogy and Petrology* **142**, 375–396.

Grove, T. L., Till, C. B. & Krawczynski, M. J. (2012). The role of H_2O in subduction zone magmatism. *Annual Review of Earth and Planetary Sciences* **40**, 413–439.

Guo, F., Nakamuru, E., Fan, W., Kobayoshi, K. & Li, C. (2007). Generation of Palaeocene adakitic andesites by magma mixing; Yanji area, NE China. *Journal of Petrology* **48**, 661–692.

Guo, J., Guo, F., Yan Wang, C. & Li, C. (2013). Crustal recycling processes in generating the early Cretaceous Fangcheng basalts, North China Craton: New constraints from mineral chemistry, oxygen isotopes of olivine and whole-rock geochemistry. *Lithos* **170–171**, 1–16.

He, L. (2014). Numerical modeling of convective erosion and peridotite–melt interaction in big mantle wedge: Implications for the destruction of the North China Craton. *Journal of Geophysical Research: Solid Earth* **119**, 2013J–10657J.

He, L. (2015). Thermal regime of the North China Craton: Implications for craton destruction. *Earth-Science Reviews* **140**, 14–26.

Heilimo, E., Halla, J. & Hölttä, P. (2010). Discrimination and origin of the sanukitoid series: Geochemical constraints from the Neoarchean western Karelian Province (Finland). *Lithos* **115**, 27–39.

Herzberg, C. (2011). Identification of source lithology in the Hawaiian and Canary Islands: implications for origins. *Journal of Petrology* **52**, 113–146.

Hollister, L. S., Grissom, G. C., Peters, E. K., Stowell, H. H. & Sisson, V. B. (1987). Confirmation of the empirical correlation of Al in hornblende with pressure of solidification of calc-alkaline plutons. *American Mineralogist* **72**, 231–239.

Hu, Z., Liu, Y., Gao, S., Liu, W., Zhang, W., Tong, X., Lin, L., Zong, K., Li, M., Chen, H., Zhou, L. & Yang, L. (2012). Improved *in situ* Hf isotope ratio analysis of zircon using newly designed X skimmer cone and jet sample cone in combination with the addition of nitrogen by laser ablation multiple collector ICP-MS. *Journal of Analytical Atomic Spectrometry* **27**, 1391–1399.

Huang, X. L. & Xu, Y. G. (2010). Thermal state and structure of the lithosphere beneath eastern China: A synthesis on basalt-borne xenoliths. *Journal of Earth Science* **21**, 711–730.

Ishimaru, S. & Arai, S. (2008). Nickel enrichment in mantle olivine beneath a volcanic front. *Contributions to Mineralogy and Petrology* **156**, 119–131.

Jahn, B., Glikson, A. Y., Peucat, J. J. & Hickman, A. H. (1981). REE geochemistry and isotopic data of Archean silicic volcanics and granitoids from the Pilbara Block, Western Australia: implications for the early crustal evolution. *Geochimica et Cosmochimica Acta* **45**, 1633–1652.

Jahn, B. M., Wu, F. Y., Lo, C. H. & Tsai, C. H. (1999). Crust–mantle interaction induced by deep subduction of the continental crust: Geochemical and Sr–Nd isotopic evidence from post-collisional mafic–ultramafic intrusions of the northern Dabie complex, central China. *Chemical Geology* **157**, 119–146.

Ji, M., Liu, J., Hu, L., Shen, L. & Guan, H. (2015). Evolving magma sources during continental lithospheric extension: Insights from the Liaonan metamorphic core complex, eastern North China Craton. *Tectonophysics* **647–648**, 48–62.

Jiang, N., Guo, J. & Chang, G. (2013). Nature and evolution of the lower crust in the eastern North China craton: A review. *Earth-Science Reviews* **122**, 1–9.

Johnson, M. C. & Rutherford, M. J. (1989). Experimental calibration of the aluminum-in-hornblende geobarometer with application to Long Valley caldera (California) volcanic rocks. *Geology* **17**, 837–841.

Kamenetsky, V. S., Elburg, M., Arculus, R. & Thomas, R. (2006). Magmatic origin of low-Ca olivine in subduction-related magmas: Co-existence of contrasting magmas. *Chemical Geology* **233**, 346–357.

Katz, R. F., Spiegelman, M. & Langmuir, C. H. (2003). A new parameterization of hydrous mantle melting. *Geochemistry, Geophysics, Geosystems* **4**, 1073.

Kelemen, P. B., Hanghøj, K. & Greene, A. R. (2003). One view of the geochemistry of subduction-related magmatic arcs, with an emphasis on primitive andesite and lower crust. In: Holland, H. D. & Turekian, K. K. (eds) *Treatise on Geochemistry, Volume 3*. Elsevier, pp. 593–659.

Kelly, R. K., Kelemen, P. B. & Jull, M. (2003). Buoyancy of the continental upper mantle. *Geochemistry, Geophysics, Geosystems* **4**, 1017.

Kessel, R., Schmidt, M. W., Ulmer, P. & Pettke, T. (2005). Trace element signature of subduction-zone fluids, melts and supercritical liquids at 120–180 km depth. *Nature* **437**, 724–727.

Kusky, T. M., Windley, B. F., Wang, L., Wang, Z., Li, X. & Zhu, P. (2014). Flat slab subduction, trench suction, and craton destruction: Comparison of the North China, Wyoming, and Brazilian cratons. *Tectonophysics* **630**, 208–221.

Laurent, O., Martin, H., Moyen, J. F. & Doucelance, R. (2014). The diversity and evolution of late-Archean granitoids: Evidence for the onset of 'modern-style' plate tectonics between 3·0 and 2·5 Ga. *Lithos* **205**, 208–235.

LBGMR (Liaoning Bureau of Geology and Mineral Resources). (1989). *Regional Geology of Liaoning Province*. Geological Publishing House.

Leake, B. E., Woolley, A. R., Arps, C., et al. (1997). Nomenclature of amphiboles: Report of the subcommittee on amphiboles of the International Mineralogical Association, commission on new minerals and mineral names. *American Mineralogist* **82**, 1019–1037.

Le Bas, M. J. (2000). IUGS reclassification of the high-Mg and picritic volcanic rocks. *Journal of Petrology* **41**, 1467–1470.

Lee, C. A., Morton, D. M., Kistler, R. W. & Baird, A. K. (2007). Petrology and tectonics of Phanerozoic continent formation: From island arcs to accretion and continental arc magmatism. *Earth and Planetary Science Letters* **263**, 370–387.

Lee, C. A., Luffi, P., Plank, T., Dalton, H. & Leeman, W. P. (2009). Constraints on the depths and temperatures of basaltic magma generation on Earth and other terrestrial planets using new thermobarometers for mafic magmas. *Earth and Planetary Science Letters* **279**, 20–33.

Lee, C. A., Luffi, P. & Chin, E. J. (2011). Building and destroying continental mantle. *Annual Review of Earth and Planetary Sciences* **39**, 59–90.

Li, C., Thakurta, J. & Ripley, E. (2012). Low-Ca contents and kink-banded textures are not unique to mantle olivine: evidence from the Duke Island Complex, Alaska. *Mineralogy and Petrology* **104**, 147–153.

Li, S. G., Xiao, Y. L., Liou, D. L., Chen, Y. Z., Ge, N. J., Zhang, Z. Q., Sun, S. S., Cong, B. L., Zhang, R. Y., Hart, S. R. & Wang, S. S. (1993). Collision of the North China and Yangtse Blocks and formation of coesite-bearing eclogites: Timing and processes. *Chemical Geology* **109**, 89–111.

Li, X. H., Liu, D. Y., Sun, M., Li, W. X., Liang, X. R. & Liu, Y. (2004). Precise Sm–Nd and U–Pb isotopic dating of the supergiant Shizhuyuan polymetallic deposit and its host granite, SE China. *Geological Magazine* **141**, 225–231.

Liu, D. Y., Nutman, A. P., Compston, W., Wu, J. S. & Shen, Q. H. (1992). Remnants of $\geq$3800 Ma crust in the Chinese part of the Sino-Korean craton. *Geology* **20**, 339–342.

Liu, J., Ji, M., Shen, L., Guan, H. & Davis, G. A. (2011). Early Cretaceous extensional structures in the Liaodong Peninsula: Structural associations, geochronological constraints and regional tectonic implications. *Science China: Earth Sciences* **54**, 823–842.

Liu, J., Shen, L., Ji, M., Guan, H., Zhang, Z. & Zhao, Z. (2013). The Liaonan/Wanfu metamorphic core complexes in the Liaodong Peninsula: Two stages of exhumation and constraints on the destruction of the North China Craton. *Tectonics* **32**, 1121–1141.

Liu, J. L., Davis, G. A., Lin, Z. Y. & Wu, F. Y. (2005). The Liaonan metamorphic core complex, Southeastern Liaoning Province, North China: A likely contributor to Cretaceous rotation of Eastern Liaoning, Korea and contiguous areas. *Tectonophysics* **407**, 65–80.

Liu, Y., Liu, H. C. & Li, X. H. (1996). Simultaneous and precise determination of 40 trace elements in rock samples using ICP-MS. *Geochimica* **25**, 552–558.

Liu, Y. S., Gao, S., Jin, S. Y., Hu, S. H., Sun, M., Zhao, Z. B. & Feng, J. L. (2001). Geochemistry of lower crustal xenoliths from Neogene Hannuoba Basalt, North China Craton: Implications for petrogenesis and lower crustal composition. *Geochimica et Cosmochimica Acta* **65**, 2589–2604.

Liu, Y. S., Gao, S., Yuan, H. L., Zhou, L., Liu, X. M., Wang, X. C., Hu, Z. C. & Wang, L. S. (2004). U–Pb zircon ages and Nd, Sr, and Pb isotopes of lower crustal xenoliths from North China Craton: insights on evolution of lower continental crust. *Chemical Geology* **211**, 87–109.

Liu, Y. S., Gao, S., Hu, Z. C., Gao, C. G., Zong, K. Q. & Wang, D. B. (2010). Continental and oceanic crust recycling-induced melt–peridotite interactions in the Trans-North China Orogen: U–Pb dating, Hf isotopes and trace elements in zircons from mantle xenoliths. *Journal of Petrology* **51**, 537–571.

Lobach-Zhuchenko, S. B., Rollinson, H., Chekulaev, V. P., Savatenkov, V. M., Kovalenko, A. V., Martin, H., Guseva, N. S. & Arestova, N. A. (2008). Petrology of a Late Archaean, highly potassic, sanukitoid pluton from the Baltic Shield: insights into Late Archaean mantle metasomatism. *Journal of Petrology* **49**, 393–420.

Lu, F. X., & Zheng, J. P. (1996). Chatacteristics of Paleozoic lithosphere and deep processes in the North China platform. In:

Chi, J. S., & Lu, F. X. (eds) *Chatacteristics of Kimberlites and Paleozoic Lithosphere in the North China Platform.* Beijing: Science Press, 215–274.

Ludwig, K. R. (2003). User's manual for Isoplot 3.00: a geochronological toolkit for Microsoft Excel. *Berkeley Geochronology Center Special Publication* **4**.

Ma, L., Jiang, S., Hofmann, A. W., Dai, B., Hou, M., Zhao, K., Chen, L., Li, J. & Jiang, Y. (2014). Lithospheric and asthenospheric sources of lamprophyres in the Jiaodong Peninsula: A consequence of rapid lithospheric thinning beneath the North China Craton? *Geochimica et Cosmochimica Acta* **124**, 250–271.

Ma, Q., Zheng, J. P., Griffin, W. L., Zhang, M., Tang, H. Y., Su, Y. P. & Ping, X. Q. (2012). Triassic 'adakitic' rocks in an extensional setting (North China): Melts from the cratonic lower crust. *Lithos* **149**, 159–173.

Ma, Q., Zheng, J., Xu, Y., Griffin, W. L. & Zhang, R. (2015). Are continental 'adakites' derived from thickened or foundered lower crust? *Earth and Planetary Science Letters* **419**, 125–133.

Mao, J., Wang, Y., Zhang, Z., Yu, J. & Niu, B. (2003). Geodynamic settings of Mesozoic large-scale mineralization in North China and adjacent areas. *Science in China, Series D: Earth Sciences* **46**, 838–851.

Martin, H. (1999). Adakitic magmas: modern analogues of Archaean granitoids. *Lithos* **46**, 411–429.

Martin, H., Smithies, R. H., Rapp, R., Moyen, J. F. & Champion, D. (2005). An overview of adakite, tonalite–trondhjemite–granodiorite (TTG), and sanukitoid: relationships and some implications for crustal evolution. *Lithos* **79**, 1–24.

McDonough, W. F. & Sun, S. S. (1995). The composition of the Earth. *Chemical Geology* **120**, 223–253.

Menzies, M. A. & Xu, Y. G. (1998). Geodynamics of the North China Craton. In: Flower, M. F. J., Chung, S., Lo, C. & Lee, T. (eds) *Mantle Dynamics and Plate Interactions in East Asia. American Geophysical Union, Geodynamic Series* **27**, 155–165.

Menzies, M. A., Fan, W. M. & Zhang, M. (1993). Palaeozoic and Cenozoic lithoprobes and the loss of >120 km of Archaean lithosphere, Sino-Korean craton, China. In: Prichard, H. M., Alabaster, T., Harris, N. B. W. & Neary, C. R. (eds) *Magmatic Processes and Plate Tectonics. Geological Society, London, Special Publications* **76**, 71–81.

Mordick, B. E., & Glazner, A. F. (2006). Clinopyroxene thermobarometry of basalts from the Coso and Big Pine volcanic fields, California. *Contributions to Mineralogy and Petrology* **152**, 111–124.

Moyen, J. (2009). High Sr/Y and La/Yb ratios: The meaning of the 'adakitic signature'. *Lithos* **112**, 556–574.

Moyen, J. (2011). The composite Archaean grey gneisses: Petrological significance, and evidence for a non-unique tectonic setting for Archaean crustal growth. *Lithos* **123**, 21–36.

Moyen, J. & Martin, H. (2012). Forty years of TTG research. *Lithos* **148**, 312–336.

Müller, R. D., Sdrolias, M., Gaina, C., Steinberger, B. & Heine, C. (2008). Long-term sea-level fluctuations driven by ocean basin dynamics. *Science* **319**, 1357–1362.

Müller, T., Dohmen, R., Becker, H. W., ter Heege, J. & Chakraborty, S. (2013). Fe–Mg interdiffusion rates in clinopyroxene: experimental data and implications for Fe–Mg exchange geothermometers. *Contributions to Mineralogy and Petrology* **166**, 1563–1576.

Nair, R. & Chacko, T. (2008). Role of oceanic plateaus in the initiation of subduction and origin of continental crust. *Geology* **36**, 583–586.

Niu, Y. (2005). Generation and evolution of basaltic magmas: Some basic concepts and a new view on the origin of Mesozoic–Cenozoic basaltic volcanism in eastern China. *Geological Journal of China Universities* **11**, 9–46.

Pallares, C., Bellon, H., Benoit, M., Maury, R. C., Aguillón-Robles, A., Calmus, T. & Cotten, J. (2008). Temporal geochemical evolution of Neogene volcanism in northern Baja California (27–30°N): Insights on the origin of post-subduction magnesian andesites. *Lithos* **105**, 162–180.

Pang, C., Wang, X., Xu, Y., Wen, S., Kuang, Y. & Hong, L. (2015). Pyroxenite-derived Early Cretaceous lavas in the Liaodong Peninsula: implication for metasomatism and thinning of the lithospheric mantle beneath North China Craton. *Lithos* **227**, 77–93.

Parman, S. W. & Grove, T. L. (2004). Harzburgite melting with and without H_2O: Experimental data and predictive modeling. *Journal of Geophysical Research: Solid Earth* **109**, B02201.

Putirka, K. D. (2008). Thermometers and barometers for volcanic systems. In: Putirka, K. D. & Tepley, F. J., III (eds) *Minerals, Inclusions and Volcanic Processes. Mineralogical Society of America and Geochemical Society, Reviews in Mineralogy and Geochemistry* **69**, 61–120.

Putirka, K. D., Mikaelian, H., Ryerson, F. & Shaw, H. (2003). New clinopyroxene–liquid thermobarometers for mafic, evolved, and volatile-bearing lava compositions, with applications to lavas from Tibet and the Snake River Plain, Idaho. *American Mineralogist* **88**, 1542–1554.

Putirka, K. D., Perfit, M., Ryerson, F. J. & Jackson, M. G. (2007). Ambient and excess mantle temperatures, olivine thermometry, and active vs. passive upwelling. *Chemical Geology* **241**, 177–206.

Qian, Q. & Hermann, J. (2010). Formation of high-Mg diorites through assimilation of peridotite by monzodiorite magma at crustal depths. *Journal of Petrology* **51**, 1381–1416.

Qian, Q. & Hermann, J. (2013). Partial melting of lower crust at 10–15 kbar: Constraints on adakite and TTG formation. *Contributions to Mineralogy and Petrology* **165**, 1195–1224.

Rapp, R. P., Shimizu, N., Norman, M. D. & Applegate, G. S. (1999). Reaction between slab-derived melts and peridotite in the mantle wedge: experimental constraints at 3·8 GPa. *Chemical Geology* **160**, 335–356.

Reimink, J. R., Chacko, T., Stern, R. A. & Heaman, L. M. (2014). Earth's earliest evolved crust generated in an Iceland-like setting. *Nature Geoscience* **7**, 529–533.

Richards, J. P. & Kerrich, R. (2007). Adakite-like rocks: their diverse origins and questionable role in metallogenesis. *Economic Geology* **102**, 537–576.

Ridolfi, F., Renzulli, A. & Puerini, M. (2010). Stability and chemical equilibrium of amphibole in calc-alkaline magmas: an overview, new thermobarometric formulations and application to subduction-related volcanoes. *Contributions to Mineralogy and Petrology* **160**, 45–66.

Roeder, P. L. & Emslie, R. F. (1970). Olivine–liquid equilibrium. *Contributions to Mineralogy and Petrology* **29**, 275–289.

Rudnick, R. L. & Gao, S. (2003). Composition of the continental crust. In: Holland, H. D. & Turekian, K. K. (eds) *Treatise on Geochemistry, Volume 3*. Elsevier, pp. 1–64.

Sato, H. (1977). Nickel content of basaltic magmas: identification of primary magmas and a measure of the degree of olivine fractionation. *Lithos* **10**, 113–120.

Shen, L., Liu, J. L., Hu, L., Guan, H. M. & Davis, G. A. (2011). The Dayingzi detachment fault system in Liaodong Peninsula and its regional tectonic significance. *Science China: Earth Sciences* **54**, 1469–1483.

Shimoda, G., Tatsumi, Y., Nohda, S., Ishizaka, K. & Jahn, B. M. (1998). Setouchi high-Mg andesites revisited: Geochemical evidence for melting of subducting sediments. *Earth and Planetary Science Letters* **160**, 479–492.

Shirey, S. B. & Hanson, G. N. (1984). Mantle-derived Archaean monzodiorites and trachyandesites. *Nature* **310**, 222–224.

Skora, S. & Blundy, J. (2010). High-pressure hydrous phase relations of radiolarian clay and implications for the involvement of subducted sediment in arc magmatism. *Journal of Petrology* **51**, 2211–2243.

Smithies, R. H. (2000). The Archaean tonalite–trondhjemite–granodiorite (TTG) series is not an analogue of Cenozoic adakite. *Earth and Planetary Science Letters* **182**, 115–125.

Sobolev, A. V., Hofmann, A. W., Sobolev, S. V. & Nikogosian, I. K. (2005). An olivine-free mantle source of Hawaiian shield basalts. *Nature* **434**, 590–597.

Straub, S. M., LaGatta, A. B., Martin-Del Pozzo, A. L. & Langmuir, C. H. (2008). Evidence from high-Ni olivines for a hybridized peridotite/pyroxenite source for orogenic andesites from the central Mexican Volcanic Belt. *Geochemistry, Geophysics, Geosystems* **9**, Q3007.

Straub, S. M., Gomez-Tuena, A., Stuart, F. M., Zellmer, G. F., Espinasa-Perena, R., Cai, Y. & Iizuka, Y. (2011). Formation of hybrid arc andesites beneath thick continental crust. *Earth and Planetary Science Letters* **303**, 337–347.

Straub, S. M., Woodhead, J. D. & Arculus, R. J. (2015). Temporal evolution of the Mariana Arc: mantle wedge and subducted slab controls revealed with a tephra perspective. *Journal of Petrology* **56**, 409–439.

Tang, Y. J., Zhang, H. F., Ying, J. F. & Su, B. X. (2013). Widespread refertilization of cratonic and circum-cratonic lithospheric mantle. *Earth-Science Reviews* **118**, 45–68.

Tatsumi, Y. (1982). Origin of high-magnesian andesites in the Setouchi volcanic belt, southwest Japan, II. Melting phase relations at high pressures. *Earth and Planetary Science Letters* **60**, 305–317.

Tatsumi, Y. (2001). Geochemical modeling of partial melting of subducting sediments and subsequent melt–mantle interaction: Generation of high-Mg andesites in the Setouchi volcanic belt, southwest Japan. *Geology* **29**, 323–326.

Tatsumi, Y. (2006). High-Mg andesites in the Setouchi Volcanic Belt, southwestern Japan: analogy to Archean magmatism and continental crust formation? *Annual Review of Earth and Planetary Sciences* **34**, 467–499.

Tatsumi, Y. (2008). Making continental crust: The sanukitoid connection. *Chinese Science Bulletin* **53**, 1620–1633.

Tatsumi, Y., Shukuno, H., Sato, K., Shibata, T. & Yoshikawa, M. (2003). The petrology and geochemistry of high-magnesium andesites at the western tip of the Setouchi Volcanic Belt, SW Japan. *Journal of Petrology* **44**, 1561–1578.

Tatsumi, Y., Suzuki, T., Kawabata, H., Sato, K., Miyazaki, T., Chang, Q., Takahashi, T., Tani, K., Shibata, T. & Yoshikawa, M. (2006). The petrology and geochemistry of Oto-Zan composite lava flow on Shodo-Shima Island, SW Japan: Remelting of a solidified high-Mg andesite magma. *Journal of Petrology* **47**, 595–629.

Wang, T., Guo, L., Zheng, Y., Donskaya, T., Gladkochub, D., Zeng, L., Li, J., Wang, Y. & Mazukabzov, A. (2012). Timing and processes of late Mesozoic mid–lower-crustal extension in continental NE Asia and implications for the tectonic setting of the destruction of the North China Craton: Mainly constrained by zircon U–Pb ages from metamorphic core complexes. *Lithos* **154**, 315–345.

Wang, X. R., Gao, S., Liu, X. M., Yuan, H. L., Hu, Z. C., Zhang, H. & Wang, X. C. (2006). Geochemistry of high-Mg andesites from the early Cretaceous Yixian Formation, western Liaoning: Implications for lower crustal delamination and Sr/Y variations. *Science in China, Series D: Earth Sciences* **49**, 904–914.

Weaver, S. L., Wallace, P. J. & Johnston, A. D. (2011). A comparative study of continental vs. intraoceanic arc mantle melting: Experimentally determined phase relations of hydrous primitive melts. *Earth and Planetary Science Letters* **308**, 97–106.

Weber, R., Wallace, P. & Dana Johnston, A. (2012). Experimental insights into the formation of high-Mg basaltic andesites in the trans-Mexican volcanic belt. *Contributions to Mineralogy and Petrology* **163**, 825–840.

Wei, G., Liang, X., Li, X. & Liu, Y. (2002). Precise measurement of Sr isotope composition of liquid and solid base using (LP) MC-ICPMS. *Geochimica* **31**, 295–299.

Weinberg, R. F. & Hasalová, P. (2015). Water-fluxed melting of the continental crust: A review. *Lithos* **212–215**, 158–188.

Willbold, M., Hegner, E., Stracke, A. & Rocholl, A. (2009). Continental geochemical signatures in dacites from Iceland and implications for models of early Archaean crust formation. *Earth and Planetary Science Letters* **279**, 44–52.

Windley, B. F., Maruyama, S. & Xiao, W. J. (2010). Delamination/thinning of sub-continental lithospheric mantle under Eastern China: The role of water and multiple subduction. *American Journal of Science* **310**, 1250–1293.

Wood, B. J. & Turner, S. P. (2009). Origin of primitive high-Mg andesite: Constraints from natural examples and experiments. *Earth and Planetary Science Letters* **283**, 59–66.

Wu, F. Y., Walker, R. J., Ren, X. W., Sun, D. Y. & Zhou, X. H. (2003). Osmium isotopic constraints on the age of lithospheric mantle beneath northeastern China. *Chemical Geology* **196**, 107–129.

Wu, F. Y., Lin, J. Q., Wilde, S. A., Zhang, X. O. & Yang, J. H. (2005a). Nature and significance of the Early Cretaceous giant igneous event in eastern China. *Earth and Planetary Science Letters* **233**, 103–119.

Wu, F. Y., Yang, J. H., Wilde, S. A. & Zhang, X. O. (2005b). Geochronology, petrogenesis and tectonic implications of Jurassic granites in the Liaodong Peninsula, NE China. *Chemical Geology* **221**, 127–156.

Wu, F. Y., Li, X. H., Yang, J. H. & Zheng, Y. F. (2007). Discussions on the petrogenesis of granites. *Acta Petrologica Sinica* **23**, 1217–1238 (in Chinese with English abstract).

Xia, Q. K., Liu, J., Liu, S. C., Kovács, I., Feng, M. & Dang, L. (2013). High water content in Mesozoic primitive basalts of the North China Craton and implications on the destruction of cratonic mantle lithosphere. *Earth and Planetary Science Letters* **361**, 85–97.

Xiao, W., Windley, B. F., Hao, J. & Zhai, M. (2003). Accretion leading to collision and the Permian Solonker suture, Inner Mongolia, China: Termination of the central Asian orogenic belt. *Tectonics* **22**, 1069.

Xiong, Q., Griffin, W., Zheng, J., O'Reilly S. & Pearson, N. (2015). Episodic refertilization and metasomatism of Archean mantle: evidence from an orogenic peridotite in North Qaidam (NE Tibet, China). *Contributions to Mineralogy and Petrology* **169**, 31.

Xiong, X. L., Adam, J. & Green, T. H. (2005). Rutile stability and rutile/melt HFSE partitioning during partial melting of hydrous basalt: Implications for TTG genesis. *Chemical Geology* **218**, 339–359.

Xu, J. F., Shinjo, R., Defant, M. J., Wang, Q. & Rapp, R. P. (2002). Origin of Mesozoic adakitic intrusive rocks in the Ningzhen area of east China: Partial melting of delaminated lower continental crust? *Geology* **30**, 1111–1114.

Xu, W. L., Hergt, J. A., Gao, S., Pei, F. P., Wang, W. & Yang, D. B. (2008). Interaction of adakitic melt–peridotite: Implications for the high-Mg# signature of Mesozoic adakitic rocks in the

eastern North China Craton. *Earth and Planetary Science Letters* **265**, 123–137.

Xu, X. S., O'Reilly, S. Y., Griffin, W. L., Zhou, X. M. & Huang, X. L. (1998). The nature of the Cenozoic lithosphere at Nushan, eastern China. In: Flower, M. F. J., Chung, S., Lo, C. & Lee, T. (eds) *Mantle Dynamics and Plate Interactions in East Asia. American Geophysical Union, Geodynamic Series* **27**, 167–196.

Xu, Y. G. (2001). Thermo-tectonic destruction of the Archaean lithospheric keel beneath the Sino-Korean Craton in China: Evidence, timing and mechanism. *Physics and Chemistry of the Earth, Part A: Solid Earth and Geodesy* **26**, 747–757.

Xu, Y. G. (2007). Diachronous lithospheric thinning of the North China Craton and formation of the Daxin'anling–Taihangshan gravity lineament. *Lithos* **96**, 281–298.

Xu, Y. G. (2014). Recycled oceanic crust in the source of 90–40 Ma basalts in North and Northeast China: Evidence, provenance and significance. *Geochimica et Cosmochimica Acta* **143**, 49–67.

Xu, Y. G., Lin, C. Y., Shi, L. B., Mercier, J. C. C. & Ross, J. V. (1995). Upper mantle geotherm for eastern China and its geological implications. *Science in China (Series B)* **38**, 1482–1492.

Xu, Y. G., Li, H. Y., Pang, C. J. & He, B. (2009). On the timing and duration of the destruction of the North China Craton. *Chinese Science Bulletin* **54**, 3379–3396.

Xu, Y. G., Zhang, H. H., Qiu, H. N., Ge, W. C. & Wu, F. Y. (2012). Oceanic crust components in continental basalts from Shuangliao, Northeast China: Derived from the mantle transition zone? *Chemical Geology* **328**, 168–184.

Yang, J. H., Wu, F. Y., Chung, S. L., Wilde, S. A. & Chu, M. F. (2004). Multiple sources for the origin of granites: Geochemical and Nd/Sr isotopic evidence from the Gudaoling granite and its mafic enclaves, northeast China. *Geochimica et Cosmochimica Acta* **68**, 4469–4483.

Yang, J. H., Wu, F. Y., Chung, S. L., Wilde, S. A. & Chu, M. F. (2006). A hybrid origin for the Qianshan A-type granite, northeast China: Geochemical and Sr–Nd–Hf isotopic evidence. *Lithos* **89**, 89–106.

Yang, J. H., Wu, F. Y., Wilde, S. A. & Liu, X. M. (2007a). Petrogenesis of Late Triassic granitoids and their enclaves with implications for post-collisional lithospheric thinning of the Liaodong Peninsula, North China Craton. *Chemical Geology* **242**, 155–175.

Yang, J. H., Wu, F. Y., Wilde, S. A., Xie, L. W., Yang, Y. H. & Liu, X. M. (2007b). Tracing magma mixing in granite genesis: *In situ* U–Pb dating and Hf-isotope analysis of zircons. *Contributions to Mineralogy and Petrology* **153**, 177–190.

Yang, J. H., Wu, F. Y., Wilde, S. A., Belousova, E. & Griffin, W. L. (2008). Mesozoic decratonization of the North China block. *Geology* **36**, 467–470.

Yang, W. & Li, S. G. (2008). Geochronology and geochemistry of the Mesozoic volcanic rocks in Western Liaoning: Implications for lithospheric thinning of the North China Craton. *Lithos* **102**, 88–117.

Yang, Y., Wu, F., Wilde, S. A., Liu, X., Zhang, Y., Xie, L. & Yang, J. (2009). *In situ* perovskite Sr–Nd isotopic constraints on the petrogenesis of the Ordovician Mengyin kimberlites in the North China Craton. *Chemical Geology* **264**, 24–42.

Yogodzinski, G. M., Kay, R. W., Volynets, O. N., Koloskov, A. V. & Kay, S. M. (1995). Magnesian andesite in the western Aleutian Komandorsky region: Implications for slab melting and processes in the mantle wedge. *Geological Society of America Bulletin* **107**, 505–519.

Yogodzinski, G. M., Brown, S. T., Kelemen, P. B., Vervoort, J. D., Portnyagin, M., Sims, K. W. W., Hoernle, K., Jicha, B. R. & Werner, R. (2015). The role of subducted basalt in the source of island arc magmas: evidence from seafloor lavas of the western Aleutians. *Journal of Petrology* **56**, 441–492.

Zhai, M. G., Guo, J. H. & Liu, W. J. (2001). An exposed cross-section of early Precambrian continental lower crust in North China craton. *Physics and Chemistry of the Earth, Part A: Solid Earth and Geodesy* **26**, 781–792.

Zhang, H. F. (2009). Peridotite–melt interaction: a key point for the destruction of cratonic lithospheric mantle. *Chinese Science Bulletin* **54**, 3417–3437.

Zhang, H. F. & Shao, J. A. (2008). Volcanic lavas of the Yixian Formation in western Liaoning province, China: Products of lower crust delamination or magma mixing? *Acta Petrologica Sinica* **24**, 37–48 (in Chinese with English abstract).

Zhang, H. F. & Yang, Y. H. (2007). Emplacement age and Sr–Nd–Hf isotopic characteristics of the diamondiferous kimberlites from the eastern North China Craton. *Acta Petrologica Sinica* **23**, 285–294 (in Chinese with English abstract).

Zhang, H. F., Sun, M., Zhou, X. H., Zhou, M. F., Fan, W. M. & Zheng, J. P. (2003). Secular evolution of the lithosphere beneath the eastern North China Craton: Evidence from Mesozoic basalts and high-Mg andesites. *Geochimica et Cosmochimica Acta* **67**, 4373–4387.

Zhang, H. F., Goldstein, S. L., Zhou, X. H., Sun, M., Zheng, J. P. & Cai, Y. (2008). Evolution of subcontinental lithospheric mantle beneath eastern China: Re–Os isotopic evidence from mantle xenoliths in Paleozoic kimberlites and Mesozoic basalts. *Contributions to Mineralogy and Petrology* **155**, 271–293.

Zhang, H. F., Zhu, R. X., Santosh, M., Ying, J. F., Su, B. X. & Hu, Y. (2013). Episodic widespread magma underplating beneath the North China Craton in the Phanerozoic: Implications for craton destruction. *Gondwana Research* **23**, 95–107.

Zhang, J., Zhao, Z., Zheng, Y. & Dai, M. (2010). Postcollisional magmatism: Geochemical constraints on the petrogenesis of Mesozoic granitoids in the Sulu orogen, China. *Lithos* **119**, 512–536.

Zhang, Y., Dong, S., Zhao, Y. & Zhang, T. (2007). Jurassic tectonics of North China: a synthetic view. *Acta Geologica Sinica* **81**, 1462–1480.

Zhao, D., Maruyama, S. & Omori, S. (2007). Mantle dynamics of Western Pacific and East Asia: Insight from seismic tomography and mineral physics. *Gondwana Research* **11**, 120–131.

Zhao, G. C., Wilde, S. A., Cawood, P. A. & Sun, M. (2001). Archean blocks and their boundaries in the North China Craton: lithological, geochemical, structural and *P–T* path constraints and tectonic evolution. *Precambrian Research* **107**, 45–73.

Zhao, Z. F., Dai, L. Q. & Zheng, Y. F. (2013). Postcollisional mafic igneous rocks record crust–mantle interaction during continental deep subduction. *Scientific Reports* **3**, 3413.

Zheng, J. P. (1999). *Mesozoic–Cenozoic mantle replacement and lithospheric thinning*. China University of Geosciences Press.

Zheng, J. P. & Lu, F. X. (1999). Mantle xenolith from kimberlites, Shandong and Liaoning: Paleozoic mantle character and heterogeneity. *Acta Petrologica Sinica* **15**, 65–74 (in Chinese with English abstract).

Zheng, J. P., Griffin, W. L., O'Reilly, S. Y., Lu, F. X., Yu, C. M., Zhang, M. & Li, H. M. (2004). U–Pb and Hf-isotope analysis of zircons in mafic xenoliths from Fuxian

kimberlites: evolution of the lower crust beneath the North China craton. *Contributions to Mineralogy and Petrology* **148**, 79–103.

Zheng, J. P., Griffin, W. L., O'Reilly, S. Y., Yang, J. S., Li, T. F., Zhang, M., Zhang, R. Y. & Liou, J. G. (2006). Mineral chemistry of peridotites from Paleozoic, Mesozoic and Cenozoic lithosphere: Constraints on mantle evolution beneath eastern China. *Journal of Petrology* **47**, 2233–2256.

Zheng, J. P., Griffin, W. L., O'Reilly, S. Y., Yu, C. M., Zhang, H. F., Pearson, N. & Zhang, M. (2007). Mechanism and timing of lithospheric modification and replacement beneath the eastern North China Craton: Peridotitic xenoliths from the 100 Ma Fuxin basalts and a regional synthesis. *Geochimica et Cosmochimica Acta* **71**, 5203–5225.

Zheng, J. P., Griffin, W. L., Ma, Q., O'Reilly, S. Y., Xiong, Q., Tang, H. Y., Zhao, J. H., Yu, C. M. & Su, Y. P. (2012). Accretion and reworking beneath the North China Craton. *Lithos* **149**, 61–78.

Zheng, J. P., Lee, C. T. A., Lu, J. G., Zhao, J. H., Wu, Y. B., Xia, B., Li, X. Y., Zhang, J. F. & Liu, Y. S. (2015). Refertilization-driven destabilization of subcontinental mantle and the importance of initial lithospheric thickness for the fate of continents. *Earth and Planetary Science Letters* **409**, 225–231.

Zhu, G., Jiang, D., Zhang, B. & Chen, Y. (2012a). Destruction of the eastern North China Craton in a backarc setting: Evidence from crustal deformation kinematics. *Gondwana Research* **22**, 86–103.

Zhu, R., Yang, J. & Wu, F. (2012b). Timing of destruction of the North China Craton. *Lithos* **149**, 51–60.

Zhu, R. X., Xu, Y. G., Zhu, G., Zhang, H. F., Xia, Q. K. & Zheng, T. Y. (2012c). Destruction of the North China Craton. *Science China: Earth Sciences* **55**, 1565–1587.

Zhu, R. X., Fan, H. R., Li, J. W., Meng, Q. R., Li, S. R. & Zeng, Q. D. (2015). Decratonic gold deposits. *Science China: Earth Sciences* **58**, 1523–1537.